iScience

CellPress
OPEN ACCESS

Article

Endothelial barrier dysfunction in systemic inflammation is mediated by soluble VE-cadherin interfering VE-PTP signaling

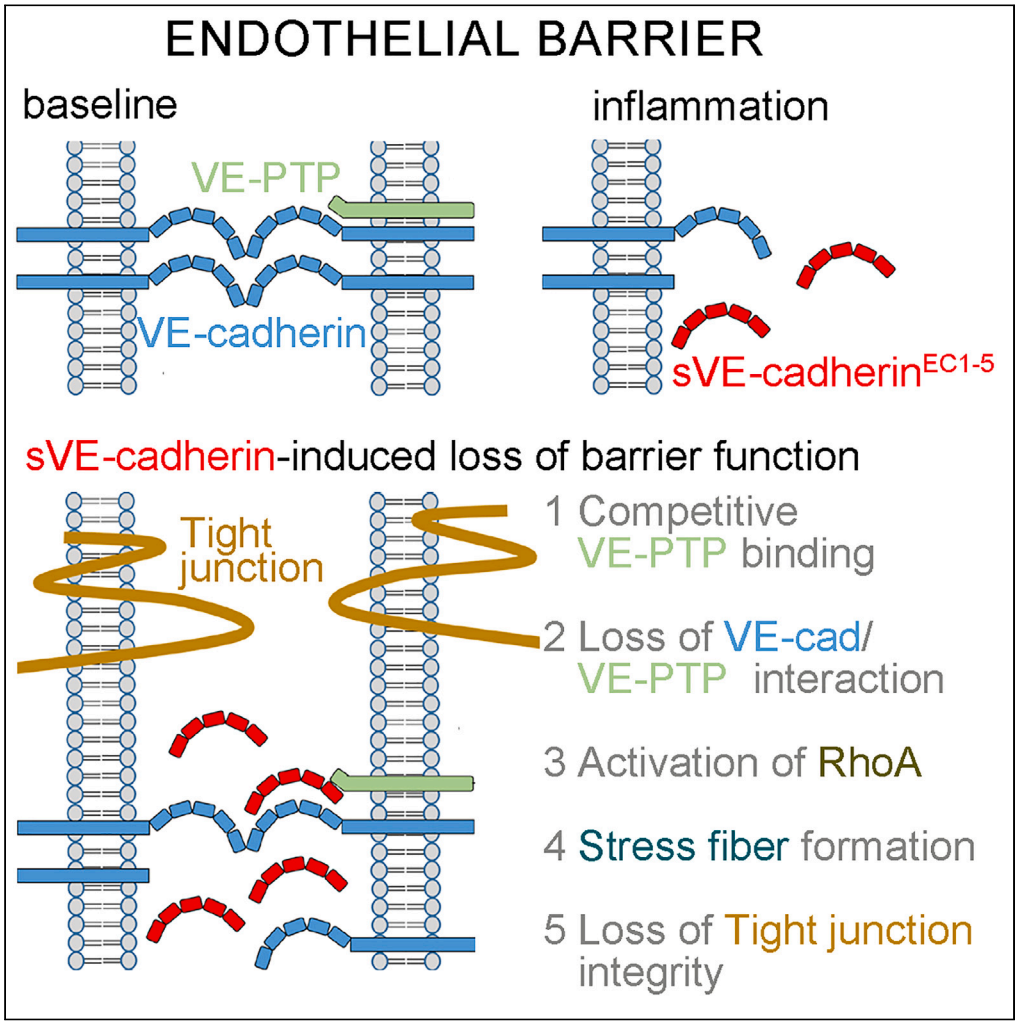

Juna-Lisa Knop, Natalie Burkard, Mahshid Danesh, ..., Jens Waschke, Sven Flemming, Nicolas Schlegel

Schlegel_N@ukw.de

Highlights

sVE-cadherin correlates with inflammation-induced endothelial barrier dysfunction

sVE-cadherin has a causative role to induce endothelial barrier dysfunction

sVE-cadherin induces barrier dysfunction by dysbalanced VE-PTP/RhoA signaling

Knop et al., iScience *26*, 108049
October 20, 2023
https://doi.org/10.1016/j.isci.2023.108049

iScience

CellPress
OPEN ACCESS

Article

Endothelial barrier dysfunction in systemic inflammation is mediated by soluble VE-cadherin interfering VE-PTP signaling

Juna-Lisa Knop,[1,7] Natalie Burkard,[1,7] Mahshid Danesh,[3] Sebastian Kintrup,[5] Thomas Dandekar,[3] Mugdha Srivastava,[4] Rebecca Springer,[1] Matthias Hiermaier,[2] Nana-Maria Wagner,[5,6] Jens Waschke,[2] Sven Flemming,[1,8] and Nicolas Schlegel[1,8,9,*]

SUMMARY

Breakdown of endothelial barrier integrity determines organ dysfunction and outcome of patients with sepsis. Increased levels of soluble vascular endothelial (VE)-cadherin fragments (sVE-cadherin) have previously been linked with inflammation-induced loss of endothelial barrier function. We provide evidence for a causative role of sVE-cadherin to induce loss of endothelial barrier function. In patients with sepsis, sVE-cadherin levels were associated with organ dysfunction and the need for volume resuscitation. Similarly, LPS-induced systemic inflammation in rats with microvascular dysfunction was paralleled by augmented sVE-cadherin levels. Newly generated recombinant human sVE-cadherin (extracellular domains EC1-5) induced loss of endothelial barrier function in both human microvascular endothelial cells *in vitro* and in rat mesenteric microvessels *in vivo* and reduced microcirculatory flow. sVE-cadherin^{EC1-5} disturbed VE-cadherin-mediated adhesion and perturbed VE-protein tyrosine phosphatase (VE-PTP)/VE-cadherin interaction resulting in RhoGEF1-mediated RhoA activation. VE-PTP inhibitor AKB9778 and Rho-kinase inhibitor Y27632 blunted all sVE-cadherin^{EC1-5}-induced effects, which uncovers a pathophysiological role of sVE-cadherin via dysbalanced VE-PTP/RhoA signaling.

INTRODUCTION

Organ failure in sepsis and in systemic inflammation have been recognized as the critical factors leading to high mortality rates in patients.[1] This is reflected by the definition of sepsis as a life-threatening organ dysfunction caused by a dysregulated host response to infection.[2] From a pathophysiological point of view, organ failure is primarily caused by the loss of microvascular function which results in tissue hypoxia.[3–5] In this context, one of the most critical steps is characterized by the breakdown of endothelial barrier function leading to the extravasation of fluid and loss of microcirculatory flow.[5–7] The underlying mechanisms are incompletely understood and therefore there is no therapeutic approach for this important and unresolved clinical problem.

Under resting conditions, endothelial cells line all blood vessels to provide a semipermeable and selectively regulated barrier.[8,9] Under inflammatory conditions, increased paracellular permeability is caused by the disruption of tight junctions (TJ) and adherens junctions (AJ) connecting neighboring endothelial cells.[8,9] The crucial determinant of endothelial barrier integrity is the 120 kDa vascular endothelial (VE)-cadherin which is a transmembrane Ca^{2+}-dependent adhesion protein. VE-cadherin is usually found as a dimer with an intra- and extracellular domain, the latter consists of 5 subdomains (EC1-5).[10] It has been reported that the integrity of endothelial barrier function is strictly dependent on the interaction between VE-cadherin and VE-protein tyrosin phosphatase (VE-PTP).[11] VE-PTP is a transmembrane protein which interacts with VE-cadherin via its extracellular domain with the EC5 domain of VE-cadherin.[12] Under conditions of inflammation, the VE-cadherin/VE-PTP interaction is impaired leading to downstream signaling which induces loss of VE-cadherin-mediated adhesion and consecutive breakdown of endothelial barrier function.[13] Therefore, this mechanism has not only been attributed to play a critical role to

[1]Department of General, Visceral, Transplantation, Vascular and Paediatric Surgery (Department of Surgery I), University Hospital Wuerzburg, Oberduerrbacherstraße 6, D-97080 Wuerzburg, Germany
[2]Chair of Vegetative Anatomy, Institute of Anatomy, Faculty of Medicine, LMU Munich, Munich, Germany
[3]University of Wuerzburg, Department of Bioinformatics, Biocenter, Am Hubland, D-97074 Wuerzburg, Germany
[4]Core Unit Systems Medicine, 97080 Würzburg, Germany
[5]University Hospital Muenster, Department of Anesthesiology, Intensive Care and Pain Medicine, Albert-Schweitzer-Campus 1, 48149 Muenster, Germany
[6]University Hospital Wuerzburg, Department of Anesthesiology, Intensive Care, Emergency and Pain Medicine, 97080 Würzburg, Germany
[7]These authors contributed equally
[8]These authors contributed equally
[9]Lead contact
*Correspondence: Schlegel_N@ukw.de
https://doi.org/10.1016/j.isci.2023.108049

Table 1. Patients' characteristics

Patient characteristics	
Sex (male/female)	11/9
Age (years)	69 ± 2.71 [39–91]
Body Mass Index (kg/m^2)	28.05 ± 1.67 [20–48]
ASA-grade	3.30 ± 0.13 [2–4]
SOFA-score	9.20 ± 0.80 [0–16]
Leukocytes (cells/nL)	21.74 ± 3.24 [6.2–58.0]
CRP (mg/dL)	20.07 ± 2.78 [4.8–57.4]
PCT (ng/mL)	23.48 ± 5.60 [4.2–100.0]
Platelets (cells/nL)	185.05 ± 20.78 [50.0–334.0]
Lactate (mmol/L)	1.68 ± 0.20 [0.5–4.0]
Crystalloid volume requirement within 24h (mL/kg)	21.86 ± 7.01 [0–114.9]
Norepinephrine requirement (μg/kg/min)	0.13 ± 0.03 [0–0.46]
Norepinephrine requirement within 24h (μg/kg)	191.05 ± 46.92 [0–810.6]
Vasopressin requirement (IE/h)	0.81 ± 0.23 [0–2.4]

The characteristics of the patients suffering from sepsis analyzed in this study are shown. Values indicated are mean values ±SD; the values in brackets indicate the range. ASA, American Society of Anesthesiologists classification; CRP, C-reactive protein; PCT, procalcitonin; SOFA, sequential organ failure assessment score.

maintain microvascular barrier function under resting conditions but also contributes to the breakdown of endothelial barrier function in systemic inflammation and sepsis.[11]

Additionally, it has been demonstrated that VE-cadherin is cleaved under inflammatory conditions leading to the release of soluble VE-cadherin (sVE-cadherin) fragments which predominately consist of the EC1-5 domains.[14,15] VE-cadherin cleavage is caused by the activation of sheddases including the specific disintegrin and metalloproteinase ADAM10.[15] Observational clinical studies have associated increased systemic sVE-cadherin levels with pathological conditions ranging from acute kidney injury[16] systemic vasculitis, chronic spontaneous urticarial[17] and systemic sepsis.[14,18] Interestingly, clinical data show that increased levels of sVE-cadherin in the blood of septic patients are associated with negative outcome of these patients.[14,16,18,19] Therefore, in a previous study we suggested sVE-cadherin as a potential clinical marker for diagnosing endothelial dysfunction in systemic inflammation and sepsis.[14] This is supported by several studies which correlated elevated sVE-cadherin levels with the onset of different inflammatory diseases.[19–21] However, it remains unclear whether increased levels of sVE-cadherin are just a marker of endothelial dysfunction or may rather be causative for the loss of endothelial barrier function. This aspect is of high clinical relevance and may expose a novel and yet unidentified pathophysiological role of sVE-cadherin to mediate or aggravate endothelial barrier dysfunction in the context of inflammation. However, currently there is no direct evidence for this hypothesis. The aim of the present study was to specifically uncover the contribution of sVE-cadherin to the loss of endothelial barrier function.

RESULTS

Soluble vascular endothelial-cadherin levels in patients with sepsis and in rat systemic inflammation correlate with the loss of endothelial barrier function

sVE-cadherin levels were assessed in critically ill patients with sepsis with a sequential organ failure assessment (SOFA) score of 9.2 ± 0.8 (range 0–16) (Table 1). Overall sVE-cadherin levels amounted 1767 ± 121 ng/mL and thus were increased when compared to patients with non-sepsis published in previous cohorts.[22,23] Correlation analyses revealed that sVE-cadherin levels in patients with sepsis were positively associated with the severity of the disease indicated by the SOFA score and with the need of crystalloid volume supply to support hemodynamics in this group of patients (Figures 1A and 1B).

Application of LPS in our previously established model of systemic inflammation in rats[4] led to inflammation-induced pulmonary edema as revealed by increased alveolar thickness compared to controls (5.38 ± 2.4 μm in controls vs. 12.67 ± 2.1 μm in the LPS group; Figures 1C and 1D). *In vivo* measurements of microvascular permeability in rat mesenteries revealed the extravasation of FITC-albumin following LPS application and reduced microvascular flow (Figures 1E and 1F). Loss of endothelial barrier function in this model was associated with increased sVE-cadherin levels compared to controls (Figure 1G). This was accompanied by an increased need of intravenous fluid supply to maintain mean arterial pressure (MAP) comparable to the observations made in patients with sepsis (Figure 1H). Accordingly dilution-induced loss of albumin was evident in LPS-treated animals (Figure 1I). In summary, clinical data from patients with sepsis and from an animal model with systemic inflammation demonstrated a close correlation between compromised endothelial barrier function and augmented sVE-cadherin levels strengthening the hypothesis that sVE-cadherin is causally involved in endothelial barrier dysfunction in systemic inflammation.

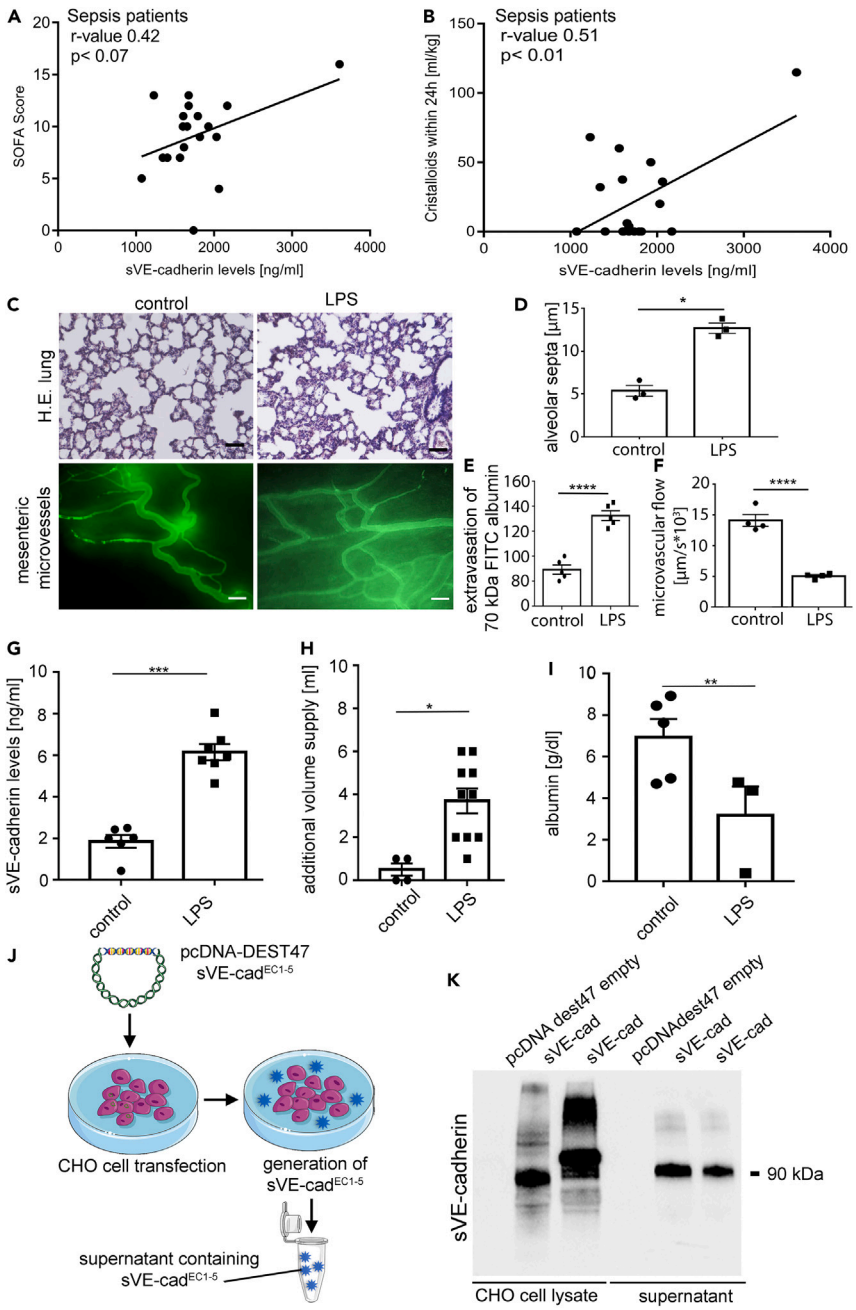

Figure 1. Augmented sVE-cadherin levels correlate with the loss of endothelial barrier function in patients with sepsis and in systemic inflammation in rats

(A) Correlation analysis between sVE-cadherin levels and sequential organ failure assessement score (SOFA) of 20 patients is shown.

(B) Correlation analysis between sVE-cadherin levels and volume resuscitation of cristalloids to stabilize the cardiovascular function of 20 patients is shown.

(C) Representative H&E-staining of rat lungs are shown with and without the application of LPS. Scale bar is 100µm (n = 3). The panels below show, representative rat mesenteric microvessels following i.v. application of FITC-albumin to document microvascular loss of endothelial barrier function are shown. Scale bar is 50µm. (n = 5).

(D) Quantitative analysis of alveolar septa thickness is shown in rats under control conditions and following LPS (*p < 0.05, n = 3, unpaired t-te4st).

(E) FITC-albumin extravasation in rat mesenteric microvessels was quantified by measuring the change of light intensity (**ΔI**) inside and outside the vessels as shown here for controls and 30 min after LPS application (****p < 0.0001, n = 5, unpaired t-test).

(F) Microcirculatory flow in rat mesenteric microvessels was investigated by the measurement of erythrocyte velocity [µm/s*10^{-3}] under control conditions and after LPS application (****p < 0.0001, n = 4 control, n = 5 LPS, unpaired t-test).

Figure 1. *Continued*

(G) ELISA-based measurements of sVE-cadherin levels [ng/ml] are shown under control conditions and following the application of LPS (***p < 0.001, n = 6 controls; n = 7 LPS, unpaired t-test).

(H) Additional volume supply [ml] to maintain mean arterial pressure ≥60 mmHg under control conditions and following the application of LPS are shown (*p < 0.05; n = 4 controls; n = 10 LPS, unpaired t-test).

(I) Albumin levels of rats at the end of the experimental procedures under control conditions and after LPS application are shown (**p < 0.01, n = 6 controls; n = 7 LPS, unpaired t-test).

(J) Schematic overview of sVE-cad^{EC1-5} generation. CHO cells were transfected with the pcDNA-DEST47 plasmid containing sVE-cad^{EC1-5} and secrete sVE-cad^{EC1-5} into the supernatant.

(K) Representative Western Blot of CHO cells and supernatants. In whole cell lysates of transfected CHO cells, a specific 90kDa protein band representing sVE-cadherin was detectable. CHO cells transfected with empty vector served as negative control. All pooled data in this figure are represented as mean ± SEM.

Soluble vascular endothelial-cadherin^{EC1-5} induces a dose-dependent loss of endothelial barrier integrity *in vitro*

To test this hypothesis we generated recombinant sVE-cadherin EC1-5. The human sequence of sVE-cadherin, which contains only the extracellular domain EC1-5, was cloned into the pcDNA-pDEST47 vector. The resulting plasmid pDEST47-sVE-cadherin^{EC1-5} was transfected into CHO cells (Figure 1J). The transfection resulted in the secretion of sVE-cadherin^{EC1-5} in cell culture supernatants which was not the case in cells transfected with pcDNA-DEST47 without the sequence of VE-cadherin^{EC1-5} (Figure 1K). Western Blot analyses revealed a protein at 90 kDa indicating the presence of the extracellular domain of VE-cadherin (sVE-cadherin^{EC1-5})[14] in supernatants and cell lysates of CHO cells transfected with pDEST47-sVE-cadherin^{EC1-5} whereas no band was detected in CHO cells transfected with pcDNA-DEST47 empty i.e., without the sequence of VE-cadherin^{EC1-5} (Figure 1K). The presence of sVE-cadherin^{EC1-5} in CHO cells transfected with pDEST47-sVE-cadherin^{EC1-5} was verified by sequencing (Figure S1), by its recognition in an ELISA that specifically detects sVE-cadherin^{EC1-5} at levels ranging at 240.22 ± 18.22 ng/mL.

Next, we tested for the effects of sVE-cadherin^{EC1-5} on endothelial barrier function using human endothelial cells (HDMECs). We used sVE-cadherin^{EC1-5} at different doses (50 ng/mL, 100 ng/mL and 130 ng/mL) and performed measurements of transendothelial resistance (TER) across confluent endothelial monolayers. As a control, the supernatant of CHO cells transfected with the pcDNA-pDEST47 vector (without the sequence of VE-cadherin^{EC1-5}) was used for *in vitro* experiments. Application of sVE-cadherin^{EC1-5} at 50 ng/mL, 100 ng/mL and 130 ng/mL significantly reduced TER after 12h, 4h and 2h compared to controls in a dose-dependent manner finally resulting in reduced TER of 0.57 ± 0.07-fold for 100 ng/mL and to 0.38 ± 0.06-fold of control for 130 ng/mL after 24h (Figure 2A). For the following experiments a dose of 130 ng/mL sVE-cadherin^{EC1-5} was chosen. In measurements of 70 kDa FITC-Dextran flux across endothelial monolayers following the application of sVE-cadherin^{EC1-5} resulted in augmented permeability coefficients (P_E) compared to controls after 1 h (1.10 ± 0.05 cm/s*10^{-6} for controls, 1.27 ± 0.08 cm/s*10^{-6} sVE-cad^{EC1-5}). Comparable results were obtained after the incubation of endothelial monolayers with 100 ng/mL LPS which increased P_E to 1.44 ± 0.06 cm/s*10^{-6} (Figure 2B). In cell viability assays we excluded that the application of sVE-cadherin^{EC1-5} on endothelial cells resulted in the induction of cell death (Figures 2C and 2D). No induction of apoptosis was detected when endothelial cells were incubated with sVE-cadherin^{EC1-5} whereas staurosporine as a known inductor of apoptosis led increased cleaved caspase-3 (Figure 2C). As revealed by immunostaining, application of sVE-cadherin^{EC1-5} resulted in a fragmented staining pattern indicating loss of VE-cadherin and intercellular gap formation (Figures 2E–2G). This was also the case for lower concentrations of sVE-cadherin^{EC1-5} incubation as revealed by immunostaining (Figure S2A). Since the anti-VE-cadherin antibody used for immunostaining was directed against the extracellular domain of VE-cadherin we performed immunostaining under the same conditions using a VE-cadherin antibody directed against the intracellular domain to exclude that the altered staining pattern resulted from a competition to the binding side. The VE-cadherin antibody directed against the intracellular domain resulted in a comparable staining pattern as the VE-cadherin antibody directed against the extracellular domain, both under control conditions and after sVE-cadherin^{EC1-5} application (Figure S2B). Fragmented VE-cadherin staining was paralleled by augmented stress fibers in F-actin staining by an overall reduction of VE-cadherin to 0.5 ± 0.1-fold of controls as revealed by Western blotting (Figures 2H and 2I).

Junctional proteins are redistributed and vascular endothelial-cadherin-mediated adhesion is reduced by soluble vascular endothelial-cadherin^{EC1-5}

To test whether the presence of sVE-cadherin^{EC1-5} interferes with the homophilic VE-cadherin transinteraction we used atomic force microscopy (AFM) where recombinant VE-cadherin molecules were covalently coupled to the cantilever tip and a mica sheet which were repeatedly brought into contact to allow the assertion of the binding probability.[24] Application of sVE-cadherin^{EC1-5} resulted in a reduction of binding activity from 61 ± 5% to 36 ± 4% (Figure 3A) which demonstrated loss of VE-cadherin-mediated adhesion by sVE-cadherin^{EC1-5}.

Proteins known to be associated with VE-cadherin such as α-, β-, and γ-catenin were also reduced from the cell borders following application sVE-cadherin^{EC1-5} of endothelial cells (Figures 3B and 3C). Similarly, the TJ protein JAM-A and TJ-associated protein ZO-1 were diminished from the cell borders following sVE-cadherin^{EC1-5} application (Figures 3B and 3C). However, their protein levels were unchanged following the incubation of endothelial cells with sVE-cadherin^{EC1-5} compared to controls in Western blot analyses (Figures 3D and S2C).

VE-PTP protein levels which is also associated with VE-cadherin were reduced in Western blot analysis following incubation with sVE-cadherin^{EC1-5} (Figures 3E and 3F). In line with this, the application of sVE-cadherin^{EC1-5} to endothelial monolayers resulted in a fragmented staining pattern of VE-PTP which showed a regular distribution at the cell periphery under control conditions (Figure 3G). In addition, reduced co-localization of VE-PTP and VE-cadherin under these conditions suggested loss of interaction between VE-cadherin and VE-PTP (Figure 4) which is critical to maintain endothelial barrier properties.[11]

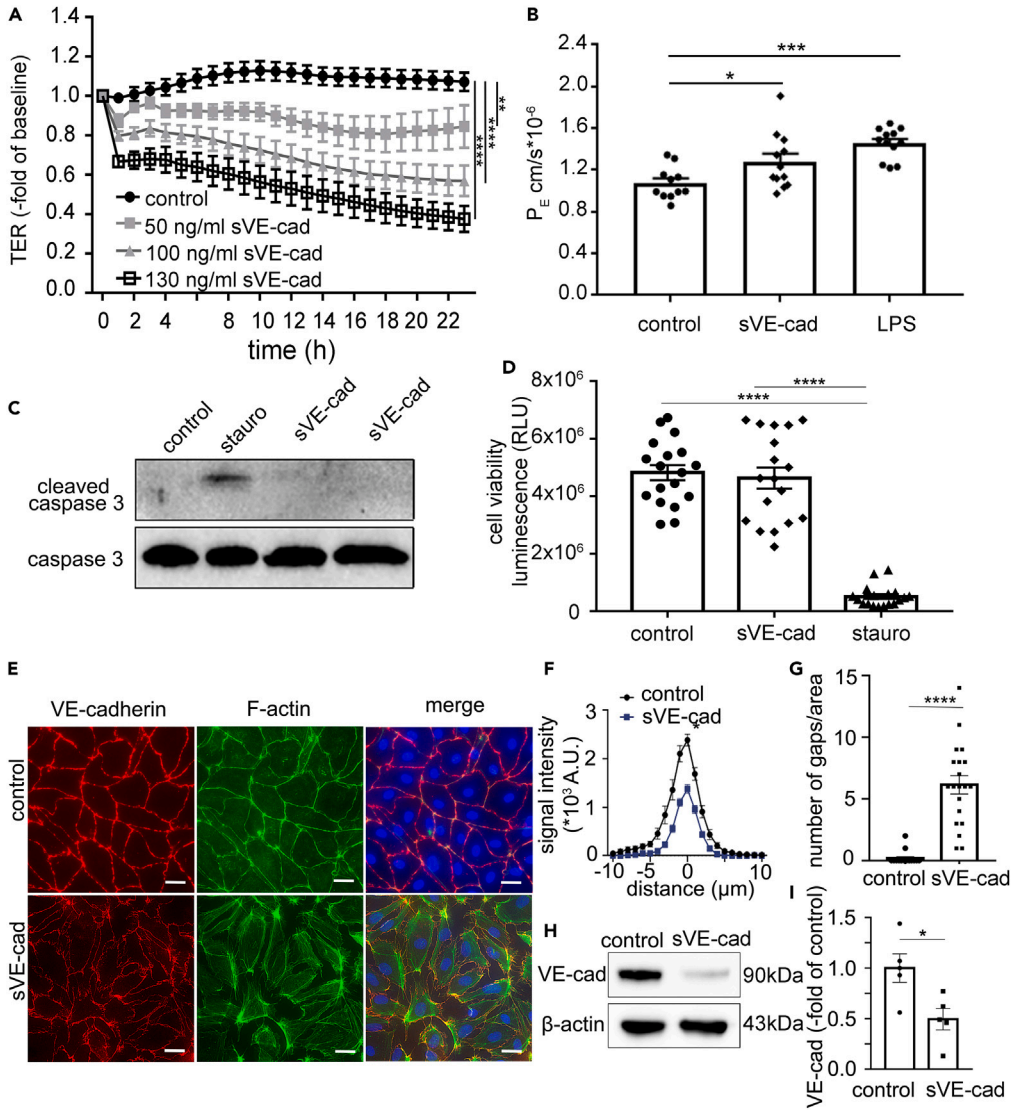

Figure 2. Generation and effects of sVE-cadherin $^{EC1-5}$ (sVE-cad^{EC1-5}) on endothelial cells

(A) Application of sVE-cad^{EC1-5} on human endothelial cells (HDMEC) resulted in a dose-dependent decrease of transendothelial electrical resistance (TER); (**p < 0.01, ****p < 0.0001, n = 4 for each condition, one-Way ANOVA with Friedman and Dunn's Test.).

(B) Permeability coefficient (P_E) measured as 70kDa FITC dextran flux across confluent (HDMEC). sVE-cad^{EC1-5} resulted in a significant increase in P_E (*p < 0.05, n = 12, one Way ANOVA with Sidak test). Lipopolysaccharide (LPS) served as a positive control (***p < 0.001, n=12 (number dots are shown in the bargraph), one Way ANOVA with Sidak Test).

(C) Representative Western Blot probed with cleaved caspase 3 antibody (used as marker of apoptosis). Only HDMEC treated with staurosporine showed a specific protein band for cleaved caspase 3. In lysates of sVE-cad^{EC1-5} treated cells, no cleaved caspase 3 was detectable; n = 4.

(D) Cell viability assay showed that sVE-cad^{EC1-5} did not induce cell death (n = 18, 1-way ANOVA). Staurosporine was used as positive control (****p < 0.0001, n = 18, 1-way ANOVA).

(E) Representative immunofluorescence staining of HDMEC treated with sVE-cad^{EC1-5} for 24h. (VE-cadherin staining in red, F-actin in green; DAPI in blue; experiment shown is representative for n > 5, scale bar is 20µm).

(F) Quantifications of VE-cadherin immunostaining of all experiments for the conditions shown in E). Application of HDMEC with sVE-cad^{EC1-5} resulted in a significant redistribution of VE-cadherin from the cell border to the cytoplasm as indicated by a flattening of the curve that measures the signal intensity at the cell border (*p < 0.05).

(G) Number of gaps/area counted in the immunostainings under control conditions and following the application of sVE-cad^{EC1-5} are shown. Gaps were counted in 20 randomly chosen areas from 5 independent experiments (****p < 0.0001; unpaired two-tailed t-test).

(H) Representative Western Blot of HDMEC cell lysate probed with VE-cadherin antibody directed against the extracellular domain of VE-cadherin. Beta actin is shown as a loading control.

(I) The protein level is significantly reduced after the application of sVE-cad^{EC1-5} (*p < 0.05, n = 5, unpaired two-tailed t-test); all pooled data in this figure are represented as mean ± SEM.

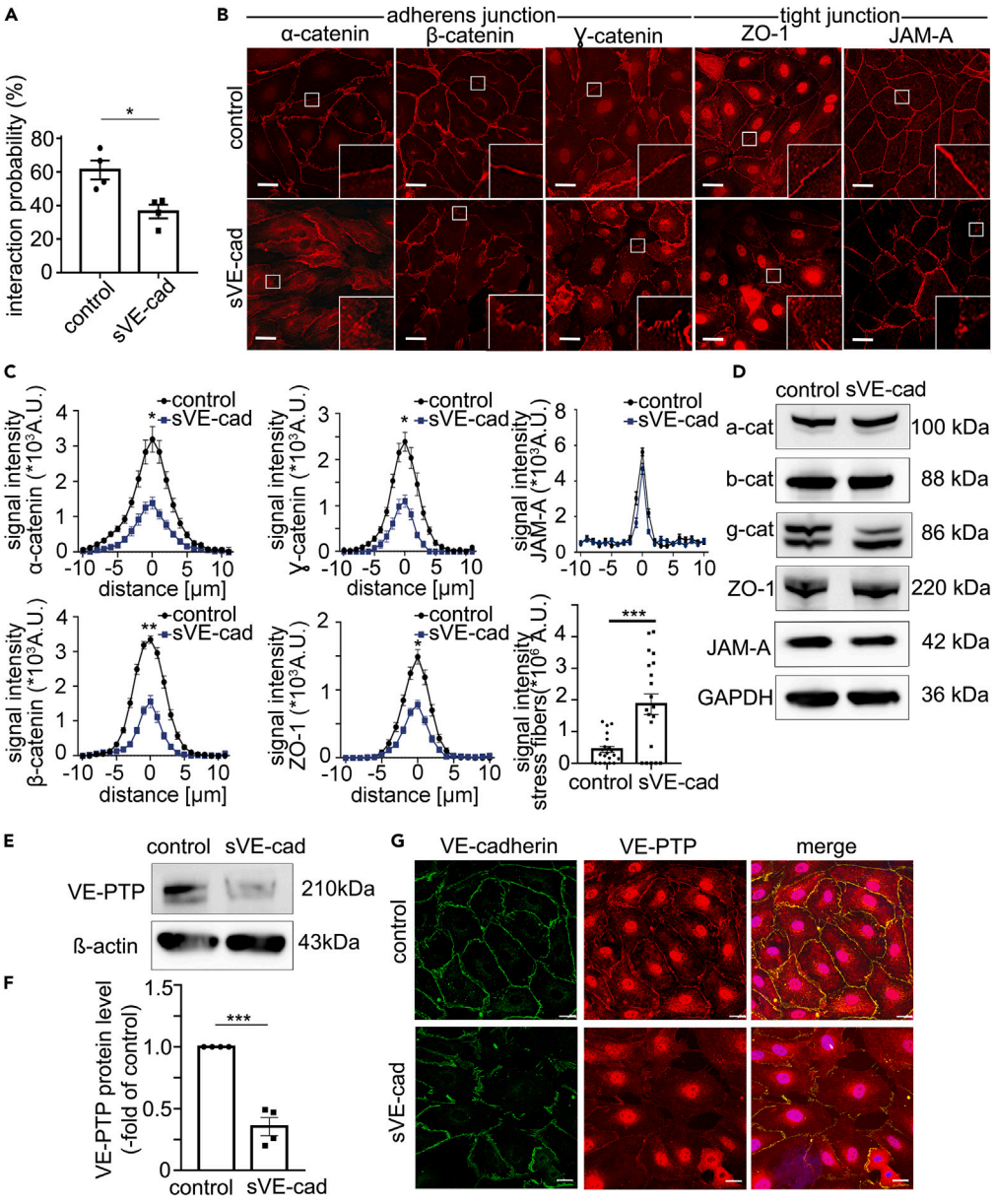

Figure 3. Cell junction proteins associated with VE-cadherin and tight-junctions are reduced at the cell border in response to sVE-cad^{EC1-5}

(A) Atomic force microscopy experiments demonstrated that the application of sVE-cad^{EC1-5} resulted in significantly reduced binding activity of VE-cadherin compared to control (*p < 0.05, n = 4, paired two-tailed t-test).

(B) Representative immunofluorescence staining for α-catenin, β-catenin, γ-catenin, ZO-1 and JAM-A of endothelial monolayer under control conditions and after 24h treatment with sVE-Cad^{EC1-5}; insets highlight the changes at the level of the junctions; n > 5 for each of the conditions; scale bar is 20 µm.

(C) Quantification of the immunostaining for the different junctional proteins α-catenin, β-catenin, γ-catenin, ZO-1 and JAM-A across 4–5 independent experiments are shown. Flattening of the curve that measures the signal intensity at the cell border indicates a loss/redistribution of the protein Quantification of F-actin staining as shown in Figure 2E) is presented to document increased staining intensity by increased stress fiber formation (*p < 0.05; **p < 0.01; ***p < 0.001, unpaired two-tailed t-test).

(D) Representative Western Blot α-catenin, β-catenin, χ-catenin, ZO-1 and JAM-A under control conditions and following the application of sVE-cad $^{EC1-5}$. GAPDH served as loading control are shown. Quantifications of all Western blots performed are presented in Figure S2C).

(E) Representative Western blot of HDMEC lysates incubated with sVE-cad^{EC1-5} showed reduced VE-PTP protein levels compared to untreated cells. Reprobing of membranes for β-actin served as loading control.

(F) Quantification of all Western blots performed for VE-PTP is shown (***p < 0.001, n = 4, unpaired two-tailed t-test).

(G) Co-immunostaining of VE-cadherin and VE-PTP showed a colocalization at the cell border under control conditions which was overall reduced following sVE-cad^{EC1-5} (n = 6; scale bar is 20 µm); all pooled data in this figure are represented as mean ± SEM.

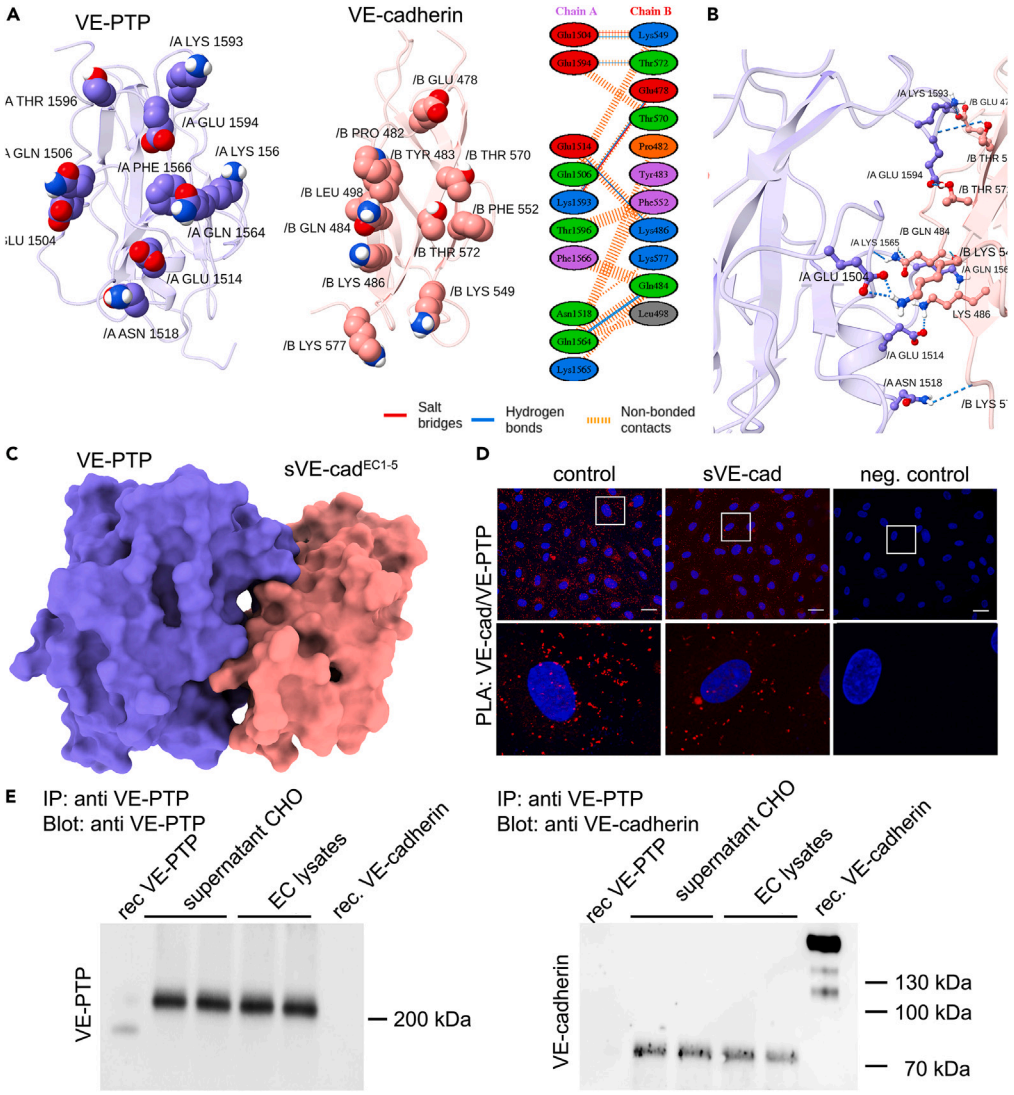

Figure 4. VE-cad^{EC1-5} binds VE-PTP leading to loss of VE-cadherin/VE-PTP interaction

(A–C) Molecular dynamic simulations revealed a direct interaction between sVE-cadherin specifically the 5th EC-domain of sVE-cadherin with the 17th domain of VE-PTP protein. For details see text.

(D) Representative pictures from proximity ligation assays (PLA) between VE-cadherin and VE-PTP are shown. Under control condition the interaction between both proteins is demonstrated as revealed by the red dots. Application of sVE-cad^{EC1-5} reduced the overall number of these spots confirming that sVE-cad^{EC1-5} interferes binding between VE-cadherin and VE-PTP. The lower pictures represent magnifications marked in the insets of the overview picture above; (n = 4; scale bar is 20 μm).

(E) Western blot following for VE-PTP (left) and VE-cadherin (right) is shown following the incubation of supernatants of CHO-cells transfected with sVE-cad^{EC-1-5} and endothelial cell lysates which were then incubated with recombinant VE-PTP. Immunoprecipitation of VE-PTP from the supernatants and cell lysates was then performed (left) and membranes were reprobed with VE-cadherin to document a direct interaction between sVE-cad^{EC1-5} and VE-PTP. The lower bands with 70–90 kDa represent sVE-cadherin (n = 3); all pooled data in this figure are represented as mean ± SEM.

Soluble vascular endothelial-cadherin^{EC1-5} interferes interaction between vascular endothelial-cadherin and vascular endothelial-protein tyrosine phosphatase

Next, we assessed whether sVE-cadherin^{EC1-5} may also bind VE-PTP to compete with the binding of VE-cadherin on the cell surface. Molecular dynamic simulations were used to test whether the 5th EC-domain of sVE-cadherin^{EC1-5} would bind VE-PTP to substantiate this hypothesis. Following the identification of active amino acids as revealed by the amount of a surface area exposed to water for more than 40%, docking simulations at defined conditions were carried out. According to this, the number of amino acids in the VE-PTP and sVE-cadherin^{EC1-5} interfaces is 10 and 11 (Figure 4A). Three salt bridges are formed between the two proteins and there are 6 hydrogen interactions and 59 non-bonded contacts between the two proteins. When studying the amount of van der Waals and electrostatic energies between the two chains during the molecular dynamics simulation the calculation of the mean value showed that the values of van der Waals and electrostatic energies are

on average equal to −202.3 and −421 kg/mol, respectively. In summary, the simulation data suggested that sVE-cadherin^{EC1-5} binds VE-PTP via the 5th EC-domain of sVE-cadherin with the 17th domain of VE-PTP protein (Figures 4B and 4C). Since this would lead to a competitive binding with cellular VE-cadherin we determined whether the application of sVE-cadherin^{EC1-5} would abrogate interaction between VE-cadherin and VE-PTP using proximity ligation assays (PLA) for VE-cadherin and VE-PTP. These experiments confirmed a close interaction between both proteins under control conditions which was reduced following sVE-cadherin^{EC1-5} supporting the simulation data that VE-PTP and sVE-adherin^{EC1-5} interact and thereby interfere with cellular VE-cadherin/VE-PTP interaction (Figure 4D). In addition, recombinant VE-PTP was incubated with the supernatant of CHO-cells transfected with sVE-cadherin^{EC1-5} or endothelial cell lysates (Figure 4E). Using anti-VE-PTP antibodies VE-PTP was immunoprecipitated. Western blot with anti-VE-cadherin antibodies resulted in a positive band at 70–90 kDa in precipitates from supernatants and endothelial cell lysates whereas precipitates from recombinant VE-PTP alone did not show any band (Figure 4E).

Vascular endothelial-protein tyrosine phosphatase activation mediates soluble vascular endothelial-cadherin^{EC1-5-} induced loss of endothelial barrier function by activating RhoA

Given that the loss of interaction between endothelial VE-cadherin and VE-PTP would result in phosphatase activation we tested whether the pharmacological inhibition of the catalytic activity of VE-PTP using AKB9778 (Razuprotafib) would attenuate the effects of sVE-cadherin^{EC1-5}.[25] As revealed by measurements of TER across endothelial monolayers co-incubation of sVE-cadherin^{EC1-5} together with AKB9778 abrogated the barrier-compromising effects of sVE-cadherin^{EC1-5} (sVE-cadherin^{EC1-5} 0.44 ± 0.08-fold of baseline; sVE-cadherin^{EC1-5} + AKB9778 0.77 ± 0.08-fold of baseline after 11 h) (Figure 5A). Application of AKB9778 alone resulted in increased TER. In the immunostaining of endothelial monolayers, VE-cadherin and VE-PTP staining patterns were largely restored, stress fiber formation was reduced and no intercellular gap formation was evident when sVE-cadherin^{EC1-5} and AKB9778 were applied together compared to incubation with sVE-cadherin^{EC1-5} incubation alone (Figure 5B). AKB9778 alone showed no changes when compared to controls (Figures S3A and S3C). The strong formation of stress fibers in the actin cytoskeleton in response to sVE-cadherin^{EC1-5} led to the hypothesis that RhoA/Rho-kinase signaling may be involved downstream of VE-PTP-mediated signaling. In Western blots for GEF-H1 we observed overall increased protein levels following the incubation of endothelial cells with sVE-cadherin^{EC1-5} (sVE-cadherin 1.43 ± 0.067-fold of control) (Figures 5C and 5D). GEF-H1 is known to promote the exchange of RhoA GDP to GTP. Using pulldown assays for active GEF-H1 we observed increased levels of active GEF-H1 after incubation with sVE-cadherin^{EC1-5} which was blunted when co-incubation with AKB9778 was carried out (Figures 5E and 5F). In line with this, RhoA activity assays measuring the amount of GTP-bound RhoA revealed a strong activation of RhoA following the application of sVE-cadherin^{EC1-5}. This was attenuated when endothelial cells were co-incubated with AKB9778 which shows that sVE-cadherin^{EC1-5}-induced RhoA activation occurs downstream to VE-PTP activation (Figures 5G and 5H). In line with this, in experiments using Rho-kinase inhibitor Y27632 sVE-cadherin^{EC1-5}-induced loss of VE-cadherin at cell borders was blocked by combined treatment of sVE-cadherin^{EC1-5} together with Y27632 in immunostaining. Stress fiber formation and intercellular gap formation observed after sVE-cadherin^{EC1-5} alone were not observed following the combined treatment of Y27632 and sVE-cadherin^{EC1-5} (Figures 5I and S3D). Accordingly, in TER measurements Y27632 in combination with sVE-cadherin^{EC1-5} attenuated the effects of sVE-cadherin^{EC1-5} on endothelial barrier function (sVE-cadherin 0.5 ± 0.01-fold of baseline; sVE-cadherin+Y27632 1.07 ± 0.01-fold of baseline after 24 h; Figure 5J). Application of Y27632 alone did not alter TER compared to controls (Y37632 1.07 ± 0.02-fold of baseline) what was also observed in immunofluorescence staining (Figure S3B).

Soluble vascular endothelial-cadherin disrupts microvascular barrier function and microcirculatory flow *in vivo*

To test the relevance of our observations *in vivo* we used the rat model that we had previously established to simultaneously monitor macrohemodynamic and microvascular changes in systemic inflammation.[4] In this model system we applied purified sVE-cadherin^{EC1-5} intravenously without the additional administration of cytokines. The sequence of EC1-5 of VE-cadherin is 86% homologue between human and rats. Simulation of the structure of EC1-5 (Figure S4) and calculation of the mean root square deviation (MRSD) between human and rat VE-cadherin using Chimera software version 2021, with Needleman-Wunsch alignment algorithm and BLOSUM-62 Matrix resulted in an RMSD of 0.306 Å (Å). An MRSD of less than about 2 Å is generally considered as very close so that this justified to use the human sVE-cadherin^{EC1-5} construct for the *in vivo* experiments in rats. Supernatants were purified via dialysis for all *in vivo* experiments so that only pure sVE-cadherin^{EC1-5} was applied in NaCl, whereas controls received purified and dialyzed supternatants from pcDNAdest47 empty in NaCl.

Due to the experimental setup, which requested a fluid replacement with 1mL 0.9% NaCl intravenously when mean arterial pressure (MAP) dropped below 60 mmHg, MAP and heart rates were not different when controls were compared to the group of animals receiving sVE-cadherin^{EC1-5} or LPS before experiments were terminated (Figures S5B and S5C). Animals after sVE-cadherin^{EC1-5} application required more additional i.v. volume application to maintain MAP above 60 mmHg (3.8 ± 1.4 mL) than controls (0.5 ± 0.3 mL compared to control). In contrast, requirement of additional volume was not observed in the group of animals that received AKB9778 + sVE-cadherin^{EC1-5} (0 ± 0 mL compared to control) (Figure 6A). Serum albumin levels at the end of the experiments were 6.9 ± 0.9 g/dL in controls and were reduced to 1.5 ± 0.3 g/dL in sVE-cadherin^{EC1-5} group, which suggested loss of microvascular barrier function and dilution due to volume replacement. This was not observed in animals treated with AKB9778 + sVE-cadherin^{EC1-5} (2.7 ± 0.7 g/dL compared to control) (Figure 6B).

Measurements of alveolar septa in H&E-stained lungs of the different groups showed pulmonary edema as revealed by increased alveolar septa to 21.03 ± 2.2 μm in animals that received sVE-cadherin^{EC1-5} compared to 5.38 ± 2.4 μm in controls. In animals treated with AKB9778 + sVE-cadherin^{EC1-5} no changes in alveolar thickness compared to controls were evident (9.8 ± 1.5 μm) (Figures 6C and 6D).

Microvascular capillary leakage was augmented to 1.5–fold of control following sVE-cadherin^{EC1-5} application as revealed by measurements of the extravasation of i.v. injection of 5 mg/100 g body weight FITC-albumin. In the group of animals receiving AKB9778 + sVE-cadherin^{EC1-5} no

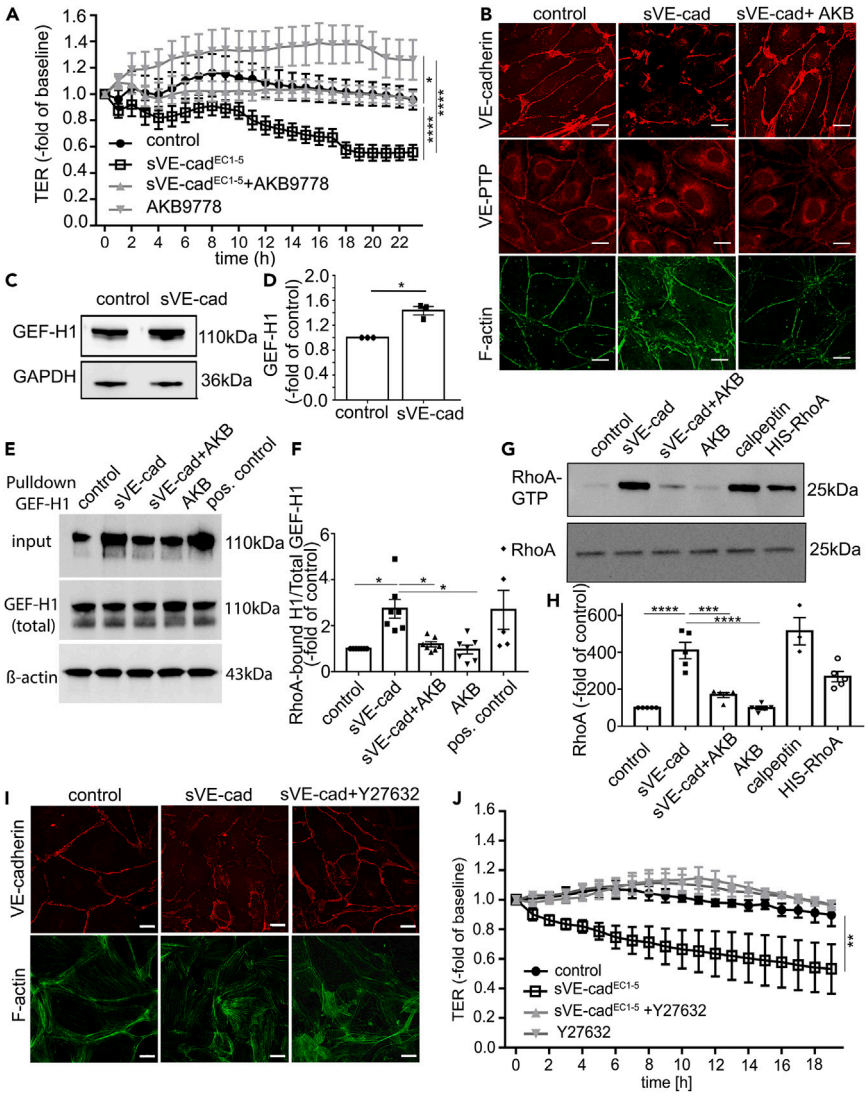

Figure 5. sVE-cad^{EC1-5} effects are mediated by the VE-PTP-dependent activation of RhoA/ROCK pathway

(A) Measurements of transendothelial electrical resistance (TER) across endothelial monolayers was carried out. Application of sVE-cad^{EC1-5} reduced TER which was blocked by AKB9778 whereas AKB9778 alone augmented TER (*p < 0.05; ****p < 0.0001; n = 12, one-Way ANOVA with Friedman and Dunn's Test).

(B) Representative immunofluorescence staining of VE-cadherin, VE-PTP and F-actin in endothelial monolayers (HDMEC) under control conditions, following incubation with sVE-cad^{EC1-5} alone or together with AKB9778 are show (n = 6, scale bar is 20 μm).

(C) Representative Western Blot and quantitative analyses of HDMEC whole cell lysates displayed increased GEF-H1 protein levels after 24h incubation with sVE-cad^{EC1-5} compared to control conditions. GAPDH served as loading control.

(D) Quantification of the Western blots performed as shown in C) is presented confirming an overall increase of GEF H1 (*p < 0.05, n = 3, unpaired two-tailed t-test).

(E) Western Blots following pulldown of activated GEF-H1 (RhoA G17) and incubation of the membranes with GEF-H1 antibodies, the total GEF-H1 levels of the input and β-actin as loading control are shown.

(F) Quantification of the experiment shown in E) revealed an increased binding between RhoA and GEF-H1 after incubation with sVE-cad^{EC1-5} compared to untreated cells which was blocked by AKB9778 (*p < 0.05, n = 6–7, ordinary 1-way ANOVA).

(G) Representative Western blot after pulldown for active GTP-bound RhoA in endothelial cells under the different conditions are shown. Calpeptin and HIS-RhoA served as internal controls. Total RhoA from endothelial lysates are shown later in discussion.

(H) Quantification of the experiment shown in (G) revealed overall augmented RhoA acitivity following the application of sVE-cad^{EC1-5} which was attenuated by co-incubation with AB9778 (***p < 0.001, ****p < 0.0001; n = 5, ordinary 1-way ANOVA).

(I) Representative immunostaining of endothelial monolayers (HDMECs) for VE-cadherin (red) and F-actin (green) are shown following incubation with sVE-cad^{EC1-5} or in combination with Rho-kinase inhibitor Y27632; n = 5; scale bar is 20 μm.

(J) TER measurements across endothelial monolayers are shown after the application of sVE-cad^{EC1-5}, after Y27632 alone or in combination with sVE-cad^{EC1-5} (**p < 0.01, n = 4, ordinary 1-way ANOVA); all pooled data in this figure are represented as mean ± SEM.

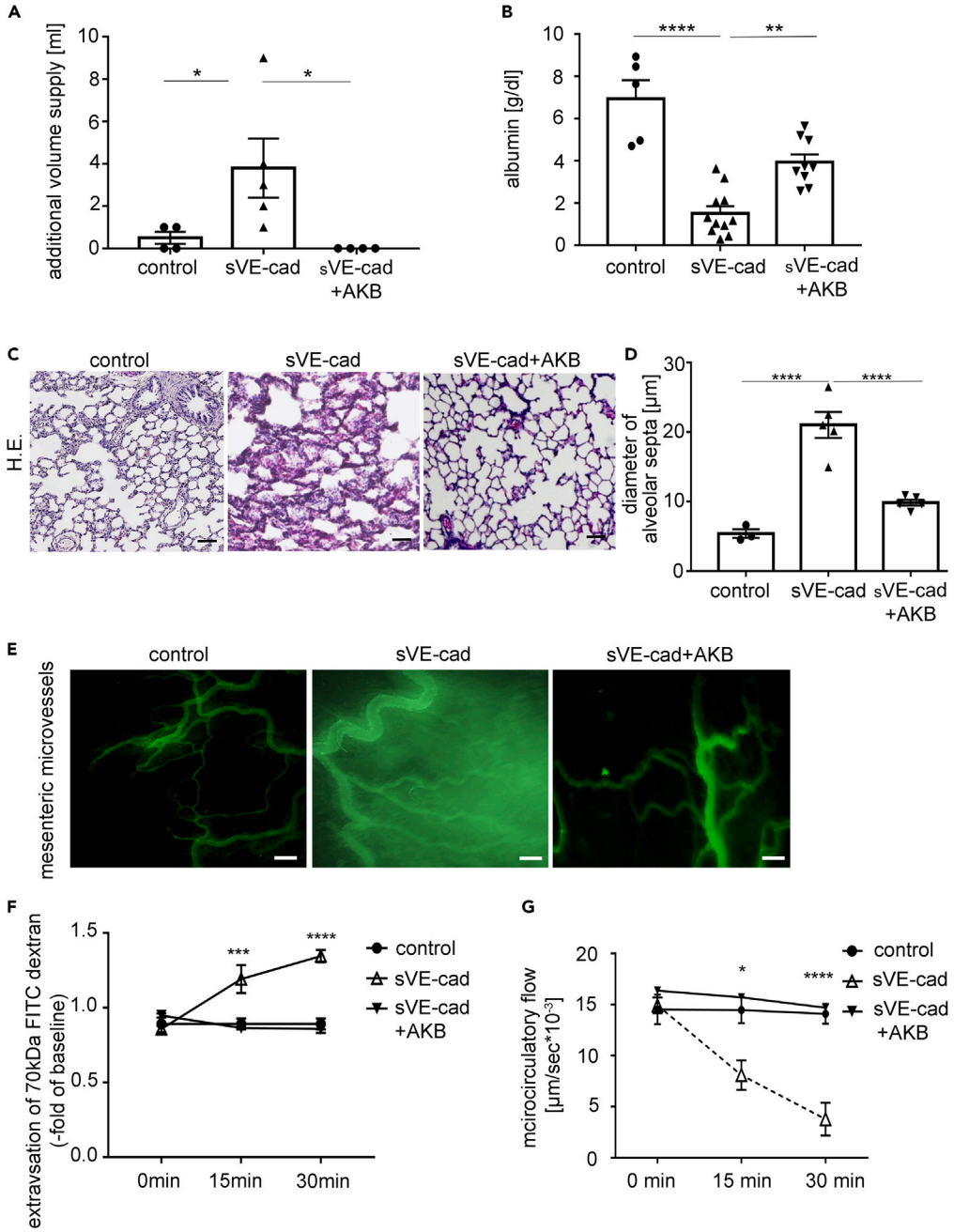

Figure 6. Application of sVE-cad^{EC1-5} induces the loss of endothelial barrier function *in vivo*

(A) Rats following the application of sVE-cad^{EC1-5} required significantly more additional volume compared to control group to maintain MAP above 60 mmHg. This was blunted by co-treatment with AKB9778 (*p < 0.05, n = 5, ordinary 1-way ANOVA).

(B) Measurement of albumin in the serum at the end of the experiment revealed decreased albumin concentration in the sVE-cad^{EC1-5} group which was not the case after the combined application of sVE-cad^{EC1-5}+AKB9778 (**p < 0.01, ****p < 0.0001, n = 5, ordinary 1-way ANOVA).

(C) Representative H.E.-stainings of lungs are shown to document the presence or absence of pulmonary edema under the different conditions. Scale bar is 100µm.

(D) Quantitative analysis of alveolar septa thickness measured from the H.E.-stainings is shown ****p < 0.0001, n = 5, ordinary 1-way ANOVA).

(E) Representative pictures of FITC-albumin extravasation in mesenteric microvessels under the different experimental conditions are shown. Scale bar is 50 µm.

(F) FITC-albumin extravasation was quantified by measuring the change of light intensity (ΔI) inside and outside the vessels (***p < 0.001, ****p < 0.0001, n = 5, ordinary 1-way ANOVA).

(G) Microcirculatory flow was investigated by the measurement of erythrocyte velocity [µm/s] (n = 5, *p < 0.01, ****p < 0.0001, n = 5, 1-way ANOVA); all pooled data presented in this figure are represented as mean ± SEM.

changes in FITC extravasation were observed (0.03 ± 0.01-fold of control after 15 and 0.03 ± 0.01-fold of control after 30 min (Figures 6E and 6F). Microvascular blood flow estimated by measurements of the velocity of erythrocytes within postcapillary mesenteric venules dropped significantly after 15min 0.56-fold of baseline after sVE-cadherin $^{EC1-5}$ application (14460.3 ± 1281 μm/s to 8087.3 ± 1447 μm/s) whereas microvascular flow remained unchanged in control animals over time (14519 ± 1434 μm/s to 14090 ± 960 μm/s). In animals that were treated with AKB9778 + sVE-cadherin^{EC1-5} loss of microvascular flow was not observed (14695 ± 875 μm/s to 14460.3 ± 1281 μm/s) (Figure 6G).

DISCUSSION

Formation of sVE-cadherin in inflammation has previously been linked with a poor prognosis in patients with sepsis.[14,16,18,19] However, it remained unexplored whether sVE-cadherin is just a result of inflammation or whether it also contributes to the vicious circle of endothelial dysfunction, loss of microvascular flow and organ failure in sepsis. This was addressed in the present study, where we provide evidence for a novel pathophysiological mechanism including dysbalanced VE-PTP-mediated RhoA signaling by which sVE-cadherin contributes to endothelial barrier disruption *in vitro* and *in vivo*. This is of high clinical relevance since specific therapies to resolve this problem are not available.

Soluble vascular endothelial-cadherin is involved in the loss of endothelial barrier function *in vivo* and *in vitro*

The clinical relevance of augmented sVE-cadherin levels is underlined by the current data from patients with sepsis in this study where sVE-cadherin levels were not only overall augmented compared to previous cohorts in healthy patients[22,23] but correlated with SOFA score and especially with the need for volume resuscitation, which indicates endothelial barrier dysfunction. Comparable observations were made when LPS was applied in a rat model to induce systemic inflammation when loss of microvascular function was associated with increased sVE-cadherin levels.

Fragments of VE-cadherin have been reported to occur as a result of pro-inflammatory stimuli in endothelial cells by shedding e.g., via ADAM10 activation.[14,15] Since the fragmentation of VE-cadherin results in loss of intercellular adhesion it is reasonable that this represents a critical hallmark to induce the loss of endothelial barrier function in inflammation.[8] The role of circulating sVE-cadherin fragments in this context remained unexplored before.

To verify the specific contribution of sVE-cadherin to the loss of endothelial barrier we cloned a recombinant sVE-cadherin fragment consisting of the EC1-5 domains which has previously been shown to be released following shedding events.[14–16] In addition to these fragments it has also been described that smaller fragments are also released in response to inflammatory stimuli.[15] We focused here on the EC1-5 fragments since they appear to represent the major fraction of VE-cadherin fragments and have been proven to be associated with a poor outcome in patients with inflammation.[14,15] As revealed by sequencing, Western blot analysis and specific commercially available ELISA measurements we confirmed that our cloning strategy truly resulted in the synthesis of sVE-cadherin EC1-5 fragments in CHO cells transfected with the vector.

Our data provide evidence that the application of sVE-cadherin alone results in the loss of endothelial barrier function in a dose-dependent manner *in vitro* and *in vivo* which was not described before. This was shown to occur to a comparable extent as when LPS was applied to endothelial cells. The fact that sVE-cadherin^{EC1-5} was applied in the absence of bacterial toxins and/or proinflammatory stimuli proves the specificity of sVE-cadherin-induced effects. However due to the experimental setup using supernatants it can be argued that other components in the supernatant (e.g., transfection reagents) may have contributed to the strong effects of sVE-cadherin observed here. We believe that this is negligible here, since we used supernatants from cells that were transfected with empty vector as control which contains the same additional components as control. In view of the fact that no changes on endothelial barrier function were observed using supernatants of cell transfected with empty vector justifies to assume that sVE-cadherin induces the effects on endothelial barrier function.

Noteworthy, the sVE-cadherin levels may be different across species and depend on the overall area of the vascular system. Therefore the specific levels of sVE-cadherin levels that are relevant to induce changes in the microcirculation *in vivo* and in patients remain unclear. Nonetheless our data *in vitro* data confirm that the presence and effects of sVE-cadherin on endothelial cells are dose-dependent.

Application of sVE-cadherin^{EC1-5} on endothelial monolayers led to loss of VE-cadherin at the cell borders and reduced total protein levels of VE-cadherin. Similarly, well known interaction partners of VE-cadherin including the junction-associated proteins α-, β-, γ-catenin that are critically involved in the proper maintenance of endothelial barrier function and are known interaction partners of VE-cadherin[26–28] as well as tight junction proteins ZO-1 and JAM-A were robustly decreased at the cell border as revealed by immunostaining. This redistribution is consistent with the disruptive effects of sVE-cadherin on endothelial barrier function.

Soluble vascular endothelial-cadherin^{EC1-5} interferes with vascular endothelial-cadherin/vascular endothelial-protein tyrosine phosphatase interaction

When considering the strong effects of sVE-cadherin^{EC1-5} on endothelial monolayers it could be assumed that the presence of sVE-cadherin induces cell death. This, however can be excluded since neither apoptosis nor reduced cell viability were observed in response to sVE-cadherin^{EC1-5} application. When focusing on the potential mechanism underlying sVE-cadherin-mediated loss of endothelial barrier function it is tempting to be content with the experiments showing that sVE-cadherin^{E1-5} directly interferes homophilic binding as revealed by atomic force microscopy measurements. However, the strong changes of VE-PTP immunostaining patterns at the cell borders following sVE-cadherin^{EC1-5} led us to test the contribution of changes in VE-PTP-dependent signaling. Since previous data point to a critical role of VE-PTP/VE-cadherin interaction for endothelial barrier stability we hypothesized whether sVE-cadherin^{EC1-5} may interfere VE-cadherin/VE-PTP interaction.[12,13] In this context, it is important to note that the interaction between both proteins is known to occur between the extracellular domain EC5 of VE-cadherin and the 17th domain of PTP protein.[12] The use of molecular simulations clearly confirmed that

sVE-cadherin^{EC1-5} may bind to VE-PTP which strengthened the hypothesis that sVE-cadherin fragments may compete with cellular VE-cadherin proteins and thereby induce endothelial barrier disruption. This is supported by PLA and immunoprecipitation experiments which confirmed the direct interaction between sVE-cadherin and VE-PTP.

A well-documented consequence of the dissociation of VE-cadherin/VE-PTP complex is the activation of different signaling pathways.[29] In line with this our experiments using AKB9778 (Razuprotafib) which blocks the catalytic activity of VE-PTP[25] showed that all functional and structural effects of sVE-cadherin^{EC1-5} application in endothelial cells were attenuated. This was also observed in the *in vivo* experiments. In a previous study VE-cadherin gene ablation did not counteract the barrier stabilizing effect of AKB9778 which led to conclusion that VE-PTP stabilizes endothelial junctions by VE-cadherin-independent mechanisms i.e., via Tie-2.[13] In addition it was shown that antibodies against the extracellular part of VE-PTP led to a dissociation and phosphorylation of Tie-2.[30] Since we observed strong stress fiber formation in response to sVE-cadherin^{EC1-5} and based on the observation that VE-PTP is involved in the regulation of RhoA activation by the inhibition of RhoGEFs[31] we tested whether RhoA signaling may be involved as a downstream mechanism.[8,9] Using immunostaining and TER measurements clearly confirmed that Rho kinase inhibitor Y27632 blunted sVE-cadherin^{EC1-5}-induced effects. In line with this RhoGEF-H1 was overall augmented and activated following the application of sVE-cadherin^{EC1-5} with a consecutive activation of GTPase RhoA. Finally, the observation that RhoA activity was prevented by AKB9778 indicates that it acts downstream of VE-PTP signaling. Thus, our data show that sVE-cadherin^{EC1-5} disrupts endothelial barrier function at least in part through VE-PTP/RhoA signaling and provide strong rationale to test VE-PTP and/or RhoA inhibitors in order to treat the endothelial barrier dysfunction associated with sepsis and possibly also other conditions.

Limitations of the study

The number of patients included in this study is too small to make definitive conclusions on the overall clinical impact of our observations. Furthermore the level of local concentration required to induce the loss of endothelial barrier remains unclear. In addition to the mechanism presented here, there may be additional signaling patterns that induce additional changes in endothelial cells that were not addressed here.

Summary and conclusion

All these findings provide evidence of a critical role of sVE-cadherin to induce vascular permeability. This has direct implications for the development of novel treatments for sepsis and other inflammatory conditions associated with increased vascular permeability. It can be speculated that the therapeutic reduction of sVE-cadherin levels could reduce severity of microvascular leakage and organ failure. This could be achieved either by preventing the shedding of VE-cadherin or by the extraction of sVE-cadherin from the blood of septic patients using dialysis. In addition, the observation that AKB9778 is effective in preventing the effects of sVE-cadherin *in vitro* and *in vivo* warrants further investigations whether this could be the long-awaited therapeutic agent to stabilize endothelial barrier dysfunction in septic patients.

STAR★METHODS

Detailed methods are provided in the online version of this paper and include the following:

- KEY RESOURCES TABLE
- RESOURCE AVAILABILITY
  - Lead contact
  - Materials availability
  - Data and code availability
- EXPERIMENTAL MODEL AND STUDY PARTICIPANT DETAILS
  - Human studies
  - *In vitro* studies
- METHOD DETAILS
  - Test reagents and antibodies
  - Cloning and generation of recombinant sVE-cadherin
  - Transfection of CHO cells
  - Co-immunoprecipitation experiments
  - Soluble VE-Cadherin enzyme-linked immunosorbent assay (ELISA)
  - Human primary cell culture of endothelial cells
  - Cell viability assay
  - Measurement of transendothelial electrical resistance (TER)
  - Permeability measurements across endothelial monolayers
  - Immunocytochemistry
  - Western blotting
  - Rho GEF-H1 binding assay
  - RhoA activity assay
  - Proximity ligation assay (PLA)
  - Atomic force microscopy (AFM) measurements with recombinant VE-cadherin-Fc

- Purification of sVE-cadherin^{EC1-5} supernatant
- Experimental set-up of *in vivo* experiments
- Randomization of animals into experimental groups
- Intravital measurement of microvascular permeability
- Evaluation of microcirculatory flow
- Histopathological analyses of lungs
- Quantification of immunostaining
- Modelling of sVE-cadherin interaction with VE-PTP

● QUANTIFICATION AND STATISTICAL ANALYSIS

SUPPLEMENTAL INFORMATION

Supplemental information can be found online at https://doi.org/10.1016/j.isci.2023.108049.

ACKNOWLEDGMENTS

rb-polyclonal VE-PTP antibody was kindly provided by D. Vestweber.

Funding: This work was supported by the Deutsche Forschungsgemeinschaft [DFG SCHL1962/4-2 to NS, DFG FL 870/2-2 to SF].

AUTHOR CONTRIBUTIONS

All authors have made substantial contributions to conception or design and approved the submission.

JLK and NB: performed experiments, analyzed data, interpreted data, involved in the conception and design of the work. Wrote the initial draft of the article.

MD: performed experiments, analyzed data, and interpreted data.

SK: performed experiments, analyzed data, and interpreted data.

TD: performed experiments, analyzed data, and interpreted data.

MS: performed experiments, analyzed data, and interpreted data.

RS: analyzed data and interpreted data.

MH: performed experiments, analyzed data, and interpreted data.

NMW: performed experiments, analyzed data, and interpreted data.

JW: performed experiments, analyzed data, and interpreted data.

SF: performed experiments, analyzed data, interpreted data, and involved in the conception and design of the work. Wrote parts of the initial draft of the article, third party funding.

NS: performed experiments, analyzed data, interpreted data, involved in the conception and design of the work, supervised the whole work, third party funding, wrote, and finalized the article and all figures.

DECLARATION OF INTERESTS

The authors declare no competing interests.

Received: March 2, 2023
Revised: August 11, 2023
Accepted: September 22, 2023
Published: September 27, 2023

REFERENCES

1. Bauer, M., Gerlach, H., Vogelmann, T., Preissing, F., Stiefel, J., and Adam, D. (2020). Mortality in sepsis and septic shock in Europe, North America and Australia between 2009 and 2019— results from a systematic review and meta-analysis. Crit. Care *24*, 239. https://doi.org/10.1186/s13054-020-02950-2.
2. Singer, M., Deutschman, C.S., Seymour, C.W., Shankar-Hari, M., Annane, D., Bauer, M., Bellomo, R., Bernard, G.R., Chiche, J.D., Coopersmith, C.M., et al. (2016). The Third International Consensus Definitions for Sepsis and Septic Shock (Sepsis-3). JAMA *315*, 801–810. https://doi.org/10.1001/jama.2016.0287.
3. Lupu, F., Kinasewitz, G., and Dormer, K. (2020). The role of endothelial shear stress on haemodynamics, inflammation, coagulation and glycocalyx during sepsis. J. Cell Mol. Med. *24*, 12258–12271. https://doi.org/10.1111/jcmm.15895.
4. Schick, M.A., Wunder, C., Wollborn, J., Roewer, N., Waschke, J., Germer, C.T., and Schlegel, N. (2012). Phosphodiesterase-4 inhibition as a therapeutic approach to treat capillary leakage in systemic inflammation. J. Physiol. *590*, 2693–2708. https://doi.org/10.1113/jphysiol.2012.232116.
5. Deutschman, C.S., and Tracey, K.J. (2014). Sepsis: current dogma and new perspectives. Immunity *40*, 463–475. https://doi.org/10.1016/j.immuni.2014.04.001.
6. Parikh, S.M. (2017). The Angiopoietin-Tie2 Signaling Axis in Systemic Inflammation. J. Am. Soc. Nephrol. *28*, 1973–1982. https://doi.org/10.1681/ASN.2017010069.
7. Ince, C., Mayeux, P.R., Nguyen, T., Gomez, H., Kellum, J.A., Ospina-Tascón, G.A., Hernandez, G., Murray, P., and De Backer, D.; ADQI XIV Workgroup (2016). The Endothelium in Sepsis. Shock *45*, 259–270. https://doi.org/10.1097/SHK.0000000000000473.
8. Radeva, M.Y., and Waschke, J. (2018). Mind the gap: mechanisms regulating the

endothelial barrier. Acta Physiol. *222*, e12860. https://doi.org/10.1111/apha.12860.

9. Spindler, V., Schlegel, N., and Waschke, J. (2010). Role of GTPases in control of microvascular permeability. Cardiovasc. Res. *87*, 243–253. https://doi.org/10.1093/cvr/cvq086.
10. Dejana, E., and Vestweber, D. (2013). The role of VE-cadherin in vascular morphogenesis and permeability control. Prog. Mol. Biol. Transl. Sci. *116*, 119–144. https://doi.org/10.1016/B978-0-12-394311-8.00006-6.
11. Vestweber, D. (2021). Vascular Endothelial Protein Tyrosine Phosphatase Regulates Endothelial Function. Physiology *36*, 84–93. https://doi.org/10.1152/physiol.00026.2020.
12. Nawroth, R., Poell, G., Ranft, A., Kloep, S., Samulowitz, U., Fachinger, G., Golding, M., Shima, D.T., Deutsch, U., and Vestweber, D. (2002). VE-PTP and VE-cadherin ectodomains interact to facilitate regulation of phosphorylation and cell contacts. EMBO J. *21*, 4885–4895. https://doi.org/10.1093/emboj/cdf497.
13. Frye, M., Dierkes, M., Küppers, V., Vockel, M., Tomm, J., Zeuschner, D., Rossaint, J., Zarbock, A., Koh, G.Y., Peters, K., et al. (2015). Interfering with VE-PTP stabilizes endothelial junctions *in vivo* via Tie-2 in the absence of VE-cadherin. J. Exp. Med. *212*, 2267–2287.
14. Flemming, S., Burkard, N., Renschler, M., Vielmuth, F., Meir, M., Schick, M.A., Wunder, C., Germer, C.T., Spindler, V., Waschke, J., and Schlegel, N. (2015). Soluble VE-cadherin is involved in endothelial barrier breakdown in systemic inflammation and sepsis. Cardiovasc. Res. *107*, 32–44. https://doi.org/10.1093/cvr/cvv144.
15. Schulz, B., Pruessmeyer, J., Maretzky, T., Ludwig, A., Blobel, C.P., Saftig, P., and Reiss, K. (2008). ADAM10 regulates endothelial permeability and T-Cell transmigration by proteolysis of vascular endothelial cadherin. Circ. Res. *102*, 1192–1201. https://doi.org/10.1161/CIRCRESAHA.107.169805.
16. Yu, W.K., McNeil, J.B., Wickersham, N.E., Shaver, C.M., Bastarache, J.A., and Ware, L.B. (2019). Vascular endothelial cadherin shedding is more severe in sepsis patients with severe acute kidney injury. Crit. Care *23*, 18. https://doi.org/10.1186/s13054-019-2315-y.
17. Chen, T., Guo, Z.-P., Wang, W.-J., Fu, L.-X., Sun, Q.-M., and Zhou, P.-M. (2017). Increased serum soluble vascular endothelial cadherin levels in patients with chronic spontaneous urticaria. Ann. Allergy Asthma Immunol. *118*, 704–709. https://doi.org/10.1016/j.anai.2017.04.013.
18. Zhang, R.Y., Liu, Y.Y., Li, L., Cui, W., Zhao, K.J., Huang, W.C., Gu, X.W., Liu, W., Wu, J., Min, D., et al. (2010). Increased levels of soluble vascular endothelial cadherin are associated with poor outcome in severe sepsis. J. Int. Med. Res. *38*, 1497–1506. https://doi.org/10.1177/147323001003800433.
19. Yu, W.K., McNeil, J.B., Wickersham, N.E., Shaver, C.M., Bastarache, J.A., and Ware, L.B. (2021). Angiopoietin-2 outperforms other endothelial biomarkers associated with severe acute kidney injury in patients with severe sepsis and respiratory failure. Crit. Care *25*, 48. https://doi.org/10.1186/s13054-021-03474-z.
20. Chen, T., Guo, Z.P., Cao, N., Qin, S., Li, M.M., and Jia, R.Z. (2014). Increased serum levels of soluble vascular endothelial-cadherin in patients with systemic vasculitis. Rheumatol. Int. *34*, 1139–1143. https://doi.org/10.1007/s00296-014-2949-7.
21. Ostrowski, S.R., Henriksen, H.H., Stensballe, J., Gybel-Brask, M., Cardenas, J.C., Baer, L.A., Cotton, B.A., Holcomb, J.B., Wade, C.E., and Johansson, P.I. (2017). Sympathoadrenal activation and endotheliopathy are drivers of hypocoagulability and hyperfibrinolysis in trauma: A prospective observational study of 404 severely injured patients. J. Trauma Acute Care Surg. *82*, 293–301. https://doi.org/10.1097/TA.0000000000001304.
22. Wrobel, T., Mazur, G., Wolowiec, D., Jazwiec, B., Sowinska, E., and Kuliczkowski, K. (2006). sVE-cadherin and sCD146 serum levels in patients with multiple myeloma. Clin. Lab. Haematol. *28*, 36–39. https://doi.org/10.1111/j.1365-2257.2006.00756.x.
23. Soeki, T., Tamura, Y., Shinohara, H., Sakabe, K., Onose, Y., and Fukuda, N. (2004). Elevated concentration of soluble vascular endothelial cadherin is associated with coronary atherosclerosis. Circ. J. *68*, 1–5. https://doi.org/10.1253/circj.68.1.
24. Heupel, W.-M., Efthymiadis, A., Schlegel, N., Muller, T., Baumer, Y., Baumgartner, W., Drenckhahn, D., and Waschke, J. (2009). Endothelial Barrier Stabilization by a Cyclic Tandem Peptide Targeting VE-Cadherin Transinteraction in Vitro and in Vivo. J. Cell Sci. *122*, 1616–1625. https://doi.org/10.1242/jcs.040212.
25. Shen, J., Frye, M., Lee, B.L., Reinardy, J.L., McClung, J.M., Ding, K., Kojima, M., Xia, H., Seidel, C., Lima e Silva, R., et al. (2014). Targeting VE-PTP activates TIE2 and stabilizes the ocular vasculature. J. Clin. Invest. *124*, 4564–4576. https://doi.org/10.1172/JCI74527.
26. Lampugnani, M.G., Corada, M., Caveda, L., Breviario, F., Ayalon, O., Geiger, B., and Dejana, E. (1995). The molecular organization of endothelial cell to cell junctions: differential association of plakoglobin, beta-catenin, and alpha-catenin with vascular endothelial cadherin (VE-cadherin). J. Cell Biol. *129*, 203–217. https://doi.org/10.1083/jcb.129.1.203.
27. Guo, M., Breslin, J.W., Wu, M.H., Gottardi, C.J., and Yuan, S.Y. (2008). VE-cadherin and beta-catenin binding dynamics during histamine-induced endothelial hyperpermeability. Am. J. Physiol. Cell Physiol. *294*, C977–C984. https://doi.org/10.1152/ajpcell.90607.2007.
28. Iyer, S., Ferreri, D.M., DeCocco, N.C., Minnear, F.L., and Vincent, P.A. (2004). VE-cadherin-p120 interaction is required for maintenance of endothelial barrier function. Am. J. Physiol. Lung Cell Mol. Physiol. *286*, L1143–L1153. https://doi.org/10.1152/ajplung.00305.2003.
29. Nottebaum, A.F., Cagna, G., Winderlich, M., Gamp, A.C., Linnepe, R., Polaschegg, C., Filippova, K., Lyck, R., Engelhardt, B., Kamenyeva, O., et al. (2008). VE-PTP maintains the endothelial barrier via plakoglobin and becomes dissociated from VE-cadherin by leukocytes and by VEGF. J. Exp. Med. *205*, 2929–2945. https://doi.org/10.1084/jem.20080406.
30. Winderlich, M., Keller, L., Cagna, G., Broermann, A., Kamenyeva, O., Kiefer, F., Deutsch, U., Nottebaum, A.F., and Vestweber, D. (2009). VE-PTP controls blood vessel development by balancing Tie-2 activity. J. Cell Biol. *185*, 657–671. https://doi.org/10.1083/jcb.200811159.
31. Juettner, V.V., Kruse, K., Dan, A., Vu, V.H., Khan, Y., Le, J., Leckband, D., Komarova, Y., and Malik, A.B. (2019). VE-PTP stabilizes VE-cadherin junctions and the endothelial barrier via a phosphatase-independent mechanism. J. Cell Biol. *218*, 1725–1742. https://doi.org/10.1083/jcb.201807210.
32. Schlegel, N., Baumer, Y., Drenckhahn, D., and Waschke, J. (2009). Lipopolysaccharide-induced endothelial barrier breakdown is cyclic adenosine monophosphate dependent *in vivo* and *in vitro*. Crit. Care Med. *37*, 1735–1743. https://doi.org/10.1097/CCM.0b013e31819deb6a.
33. Baumer, Y., Drenckhahn, D., and Waschke, J. (2008). cAMP induced Rac 1-mediated cytoskeletal reorganization in microvascular endothelium. Histochem. Cell Biol. *129*, 765–778. https://doi.org/10.1007/s00418-008-0422-y.
34. Schlegel, N., Burger, S., Golenhofen, N., Walter, U., Drenckhahn, D., and Waschke, J. (2008). The role of VASP in regulation of cAMP- and Rac 1-mediated endothelial barrier stabilization. Am. J. Physiol. Cell Physiol. *294*, C178–C188.
35. Burkard, N., Meir, M., Kannapin, F., Otto, C., Petzke, M., Germer, C.T., Waschke, J., and Schlegel, N. (2021). Desmoglein2 Regulates Claudin2 Expression by Sequestering PI-3-Kinase in Intestinal Epithelial Cells. Front. Immunol. *12*, 756321. https://doi.org/10.3389/fimmu.2021.756321.
36. Sielenkämper, A.W., Meyer, J., Kloppenburg, H., Eicker, K., and Van Aken, H. (2001). The effects of sepsis on gut mucosal blood flow in rats. Eur. J. Anaesthesiol. *18*, 673–678. https://doi.org/10.1046/j.1365-2346.2001.00905.x.
37. Wunder, C., Brock, R.W., McCarter, S.D., Bihari, A., Harris, K., Eichelbrönner, O., and Potter, R.F. (2002). Inhibition of haem oxygenase activity increases leukocyte accumulation in the liver following limb ischaemia-reperfusion in mice. J. Physiol. *540*, 1013–1021. https://doi.org/10.1113/jphysiol.2001.015446.
38. Waschke, J., Drenckhahn, D., Adamson, R.H., Barth, H., and Curry, F.E. (2004). cAMP protects endothelial barrier functions by preventing Rac-1 inhibition. Am. J. Physiol. Heart Circ. Physiol. *287*, H2427–H2433. https://doi.org/10.1152/ajpheart.00556.2004.
39. Bekker, A.Y., Ritter, A.B., and Durán, W.N. (1989). Analysis of microvascular permeability to macromolecules by video-image digital processing. Microvasc. Res. *38*, 200–216. https://doi.org/10.1016/0026-2862(89)90028-9.

STAR★METHODS

KEY RESOURCES TABLE

REAGENT or RESOURCE	SOURCE	IDENTIFIER
Antibodies		
VE-cadherin extracellular domain	R&D Systems	RRID:AB_2260374; MAB9381
VE-cadherin intracellular domain	Santa Cruz	RRID:AB_2077957; sc-9989
ZO-1	Millipore	RRID:AB_10807434;AB2272
α-catenin	Thermofisher	RRID:AB_2533974; 71-1200
β-catenin	Invitrogen	RRID: AB_2533982; 71-2700
γ- catenin	Cell Signaling	RRID:AB_823448; 2309
VE-PTP	Novus Bio	CatNo NBP2-88892
VE-PTP	D. Vestweber	
VE-PTP	Antikörper online	ABIN1860364
cleaved caspase-3 (Asp175)	Cell Signaling	RRID:AB_2341188; CatNo 9661
caspase antibody	cell signalling	RRID:AB_331439; CatNo 9662S
GAPDH	Sigma-Aldrich	RRID:AB_1078992; G9295
JAM-A	Invitrogen	RRID:AB_2533241; 36-1700
β-actin	Sigma-Aldrich	RRID:AB_262011; A3854
gam pox	Dianova	RRID:AB_10015289; 115-035-003
garb pox	Dianova	RRID:AB_2313567; 111-035-003
Dam Alexa Fluor 488	Invitrogen	RRID:AB_2535787; A-21201
darb Alexa Fluor 488	Invitrogen	RRID:AB_2535792; A-21206
gam cy3	Dianova	RRID:AB_2338680; 115-165-003
RhoGEF-H1	Abcam	RRID:AB_2818944; ab155785
garb cy3	Dianova	RRID:AB_2338000; 111-165-003
Bacterial and virus strains		
pcDNA-DEST47	Thermo Fisher Scientific	12281010
Biological samples		
Blood from sepsis patients	This paper	
Chemicals, peptides, and recombinant proteins		
sVE-cadherin^{EC1-5}	This paper	
Gateway LR Clonase II enzyme mix	Thermo Fisher Scientific	11791020
Lipofectamine LTX reagent	Thermo Fisher Scientific	15338100
Halt proteinase inhibitor cocktail	Thermo Fisher Scientific	Ref.: 78438
RIPA-buffer	Thermo Fisher Scientific	89900
Triton X-100	Carl Roth GmbH + Co. KG	3051.2
Razuprotafib (AKB)	Hycultec	Hy-109041
Y27632	Sigma Aldrich	688000
Critical commercial assays		
sVE-cadherin ELISA (human)	R&D Systems	DCADV0
sVE-cadherin ELISA (rat)	MYBioSource	MBS2511473
Immunoprecipitation Starter Pack	GE Healthcare	Y2-VW-17-6002-35
CellTiter-Glo® 2.0 Assay	Promega	CatNo G9241
GEF-H1 RhoA G17 agarose beads	Abcam	ab211183

(*Continued on next page*)

Continued		
REAGENT or RESOURCE	SOURCE	IDENTIFIER
Rho Activation Assay Biochem Kit	Cytoskeleton	CatNo BK036-S
Duolink Proximity Ligation Assay	Sigma Aldrich	DUO92101
Deposited data		
Original Western Blot Data	https://doi.org/10.17632/ns3b3cd8jv.1	Mendeley Data
Original Datasets	https://doi.org/10.5281/zenodo.8320820	ZENODO
Experimental models: Cell lines		
sCHO cells	ATCC	PTA 3765
Human Dermal Microvascular Endothelial Cells	Promocell	CatNo C-12262
Experimental models: Organisms/strains		
Sprague-Dawley rats	Janvier	
Software and algorithms		
GraphPad Prism		
chemiDoc Touch Image Lab		
ImageJ		
VisiView		
BZII-Analyzer		

RESOURCE AVAILABILITY

Lead contact

Further information and requests for resources and reagents should be directed to and will be fulfilled by the lead contact Prof. Dr. Nicolas Schlegel (Schlegel_N@ukw.de).

Materials availability

The newly generated sVE-cadherin EC1-5 plasmid (Figure S1A) can be requested by contacting the lead contact.

Data and code availability

- Original western blot images have been deposited at Mendeley and are publicly available as of the date of publication. The DOI is listed in the key resources table. Microscopy data reported in this paper will be shared by the lead contact upon request.
- All original code has been deposited at Zenodo and is publicly available as of the date of publication. DOIs are listed in the key resources table.
- Any additional information required to reanalyze the data reported in this paper is available from the lead contact upon request.

EXPERIMENTAL MODEL AND STUDY PARTICIPANT DETAILS

Human studies

Septic patients were recruited upon diagnosis of sepsis on the intensive care unit and written informed consent was obtained. Study approval was obtained by the Ethics Committee of the University Hospital Münster (2019-494-f-S). Blood was drawn, centrifuged and plasma was stored pending analysis. sVE-cadherin levels were obtained by ELISA (R&D Systems) as described below.

Information about gender, sex and age are listed in Table 1. In these critically ill patients no influence of sex and gender on sVE-cadherin levels is assumed. All participants were European Caucasian. The socioeconomic status was not evaluated since it was not relevant for this study.

Animal experiments

All animal experiments were approved by the animal care committee (laboratory animal care and use committee of the district of Unterfranken, Germany) by the Regierung von Unterfranken (AZ 2-1241), Germany. All animal experiments performed conform to the guidelines from Directive 2010/64/EU of the European Parliament on the protection of animals used for scientific purposes which also conform to the ARRIVE guidelines. Experiments were performed on male Sprague-Dawley rats (n=20; aged 5-7 weeks, 200-250 g; Janvier, 53940 Le Genest Saint Isle, France). Male rats were used to obtain comparable results and to exclude female hormone-related effects on systemic inflammation and microvascular leakage. Animals were kept under conditions that conformed to the National Institutes of Health "Guide for the Care and

Use of Laboratory Animals". All rats were maintained on a standard diet and water ad libitium for 12 h day and night cycles. Animals were not fasted prior to the procedure.

In vitro studies

Human endothelial cells used in this study were obtained commercially (HDMEC; Promocell, Heidelberg, Germany). The preparation of the endothelial cells conforms to the Declaration of Helsinki. According to the manufacturers information the cells derived from adult donors from foreskin or from different locations of the adult skin (https://promocell.com/product/human-dermal-microvascular-endothelial-cells-hdmec). Based on this, endothelial cells derived from both sex and gender and led to similar results so that an influence on the results of sex and gender in data obtained from these cells is not likely.

METHOD DETAILS

Test reagents and antibodies

The following primary antibodies were used for Western blot (WB) or immunofluorescent (IF) staining as indicated below: Antibody against VE-cadherin extracellular domain (WB 1:1000, IF 1:50, R&D Systems, MAB9381), antibody against VE-cadherin intracellular domain (WB 1:1000, Santa Cruz, sc-9989), ZO-1 (WB 1:500, IF 1:50, Millipore, AB2272), α-catenin (WB 1:500, IF 1:50, Thermofisher, 71-1200), β-catenin (WB 1:1000, IF 1:50, Invitrogen, 71-2700), γ- catenin (WB 1:500, IF 1:50, Cell Signalling, 2309), rb-polyclonal VE-PTP against c-terminus (0.5 μg/ml, kindly provided by Dietmar Vestweber, Münster, Germany), VE-PTP (IF 1:100, Novus Bio, CatNo NBP2-88892), cleaved caspase-3 (Asp175) antibody (WB 1:600, Cell Signaling, CatNo 9661), caspase antibody (WB 1:1000, cell signalling, CatNo 9662S), GAPDH (WB 1:5000, Sigma-Aldrich, G9295), β-actin (WB 1:3000, Sigma-Aldrich, A3854). JAM-A (WB 1:500, IF 1:100, Invitrogen 36-1700).The following horseradish peroxidase-labeled IgG secondary antibodies were used for Western blotting: gam pox (WB 1:3000, Dianova, 115-035-003), garb pox (WB 1:3000, Dianova, 111-035-003), dam Alexa Fluor 488 (1:200, Invitrogen, A-21201), darb Alexa Fluor 488 (1:200, Invitrogen, A-21206), gam cy3 (1:600, Dianova, 115-165-003), garb cy3 (1:600, Dianova, 111-165-003).

Cloning and generation of recombinant sVE-cadherin

sVE-cadherin^{EC1-5} was secreted into the supernatant by CHO cells that were transfected with the pcDNA-DEST47 containing the sequence of VE-cadherin EC1-5. Cloning was performed according to manufacturer's protocol (Gateway cloning system, Thermo Fisher Scientific, Waltham MA, USA). First, the coding sequence of EC1-5 of human VE-cadherin was amplified using cDNA from HUVEC cells as a template. The used primer pairs were designed according the Uniprot Reference for human VE-cadherin (extracellular domain) (P33151 (CADH5_HUMAN)). The Gateway Technology uses the lambda recombination system to facilitate transfer of heterologous DNA sequences (flanked by modified *att* sites) between vectors. Two recombination reactions constitute the basis of the Gateway Technology. The first BP reaction facilitates recombination of an *att*B substrate (*att*B-PCR product of VE-cadherin EC1-5) with an *att*P substrate (donor Vector: pENTR/SD-D-TOPO vector (Thermo Fisher Scientific, Waltham MA USA)) to create an *att*L-containing ENTRY clone. The *att*B PCR primer were designed according to manufacturer's protocol (Gateway cloning system, Thermo Fisher Scientific, Waltham MA, USA). Forward primer contains Shine-Dalgarno and Kozak consensus sequence for protein expression in both *E.coli* and mammalian cells. (Forward primer: 5′ GGG GAC AAG TTT GTA CAA AAA AGC AGG CTT CGA AGG AGA TAG AAC CAT GAT GCA GAG GCT CAT GAT GCT C 3′; Reverse primer: 5′ GGG GAC CAC TTT GTA CAA GAA AGC TGG GTC GTC AAA CTG CCC ATA CTT GAC 3′).

For the BP Recombination reaction, 10 μl of the amplified *att*B-PCR product, 2 μl pDONOR vector, 5 μl BP clonase reaction buffer, and 4 μl BP clonase enzyme is combined in a 1.5 ml microcentrifuge tube. After an incubation of 1 h at 25°C, 2 μl Proteinase K is added and again incubated for 1 h at 37°C. The created ENTRY clone (pENTR/SD-D-TOPO vector with VE-cadherin EC1-5 inserted) was transformed in competent *E.coli* cells, antibiotica selected and analyzed via colony PCR. The positive transformants containing the sequence of human VE-cadherin EC1-5 were used for the second recombination reaction, the LR reaction. The LR reaction facilitates recombination of an *att*L substrate (the created ENTRY clone) with an *att*R substrate (destination vector pcDNA-DEST 47 (Thermo Fisher Scientific, Waltham MA, USA)) to create an *att*B-containing expression clone. The Gateway pcDNA-DEST 47 Vector is a destination vector for cloning and exression of GFP fusion proteins in mammalian cells. Genes (VE-cadherin EC 1-5) in the created ENTRY clone are transferred to the destination vector backbone by mixing the DNAs with the Gateway LR Clonase II enzyme mix (Thermo Fisher Scientific, Waltham MA, USA). In detail: for the LR Recombination reaction, 10 μl of the created ENTRY clone, 2 μl destination vector, 4 μl 5X LR clonase reaction buffer, and 4 μl LR clonase enzyme is combined in a 1.5 ml microcentrifuge tube. The resulting recombination reaction is then transformed into *E.coli* and the expression clone selected. After an incubation of 1 h at 25°C, 2 μl Proteinase K is added and again incubated for 1 h at 37°C. The created destination vector (pcDNA-DEST47 vector with VE-cadherin EC1-5 inserted) was transformed in competent *E.coli* cells, antibiotica selected and analyzed via colony PCR. The positive transformants were used for all the following experiments.

Transfection of CHO cells

Transfection reagents were prepared as follows: Reaction mix A containing 600 μl Opti-MEM (Thermo Fisher Scientific, Waltham MA, USA; Ref.: 31985062) and 24 μl Lipofectamine LTX reagent (Thermo Fisher Scientific, Waltham MA, USA, Ref: 15338100) and reaction mix B containing 700 μl Opti-MEM, 14 μl Plus reagent and 8 μg of the pcDNA-DEST47-EC1-5 plasmid were mixed and incubated for 5 minutes at room temperature. As a control for all *in vitro* experiments, CHO cells were transfected with pcDNA-DEST47 without the sequence of

VE-cadherin $^{EC1-5}$. The subsequent steps were all the same like the CHO cells transfected with the pcDNA-DEST47-EC1-5. Thereafter, CHO cells (70 % confluent) at transfection day were incubated with 700 µl medium and 300 µl transfection mixture. CHO cells were obtained from ATCC (PTA 3765).

Three to four days after transfection the supernatant was taken and Halt proteinase inhibitor cocktail (Thermo Fisher Scientific, Waltham MA, USA; Ref.: 78438) was added. The supernatant was stored at 4°C until usage. The concentration of EC1-5 in the supernatants was measured using sVE-cadherin ELISA.

For control experiments cells CHO cells were transfected with the pcDNA-pDEST47 vector (without the sequence of VE-cadherin^{EC1-5}) and supernatant was collected. This supernatant was used as control in the *in vitro* experiments. To ensure that there were no interfering proteins in the supernatant, coomassie staining was performed. Coomassie blue dye is commonly used to stain unspecific every existing protein in SDS-PAGE gels.

Co-immunoprecipitation experiments

Cells were seeded on 6-well plates. Monolayer cells at confluency were harvested in RIPA-buffer (ThermoFisher; CatNo 89900). Samples were steamed for 1min and centrifuged for 15min at 15.000g and 4°C. Total protein concentration was determined by measuring absorbance at 280nm.

The Co-IP experiments were done using the immunoprecipitation Starter Pack (GE Healthcare, Germany, Ref Y2-VW-17-6002-35). The amount of 300-600 µg protein was used. After an initial pre-clearing step of one hour at 4°C (500µl of whole cell lysate with respectively 25µl protein G / A sepharose beads), antigens were coupled overnight at 4°C to 2.5 µg purified antibody rabbit anti-VE-PTP (Antikoerper online, Aachen, Germany, CatNo ABIN1860364). Protein-antibody complexes were precipitated with a mix of 25µl protein A and G sepharose beads for one hour at 4°C. The beads were washed three times with isotonic salt buffer (RIPA-buffer, Thermo Fisher, CatNo 89900), once with wash-buffer (50 mM TRIS, pH 8) and suspended in 50µl Laemmli buffer. After denaturation for 5min at 95°C and a following centrifugation step, the supernatant was analysed by western Blot analyses as described above. Detection was performed with mouse anti-VE cadherin 1:500 (R&D Systems, Wiesbaden, Germany, CatNO MAB9381). Optical densities (OD) were quantified in each Western Blot using Image Lab ChemicDoc Touch (Bio-Rad Laboratories GmbH, Munich, Germany) for statistical evaluation.

Soluble VE-Cadherin enzyme-linked immunosorbent assay (ELISA)

ELISA-based quantification of soluble VE-cadherin in cell culture supernatants (R&D Systems, Wiesbaden-Nordenstadt, Germany, DCADV0) and rat blood (MYBioSource, San Diego, USA MBS2511473) samples was performed by using VE-cadherin ELISA according to manufacturer's instructions. As maintained by the company the antibody in this ELISA recognizes epitopes between Asp48 and Gln593 which correspond to the extracellular domain of VE-cadherin.[14]

Human primary cell culture of endothelial cells

We used Human Dermal Microvascular Endothelial Cells (HDMEC; Promocell, Heidelberg, Germany, CatNo C-12262) that were described previously to be a suitable model to study microvascular endothelial barrier regulation *in vitro*.[14,32] Cells were used from passages 1 to 7 and grown in endothelial growth medium containing supplement mix and were passaged using Detach kit-30 (both Promocell). Culture confluency was checked by daily microscopy.

Cell viability assay

For measuring cell viability CellTiter-Glo® 2.0 Assay (Promega, Madison; USA; CatNo G9241), a luminescence-based cell viability assay was used. The number of viable cells in culture is determined by quantification of the amount of ATP present. The experimental set-up was designed and executed according to the manufacturer's protocol. In brief, cells were grown on opaque-walled multiwall plates, CellTiter-Glo® 2.0 reagent was added, and luminescence signal was measured. The luminescence signal is proportional to the amount of ATP present; the amount of ATP is directly proportional to the number of viable cells present in culture. Data were normalized to the controls of each experiment.[14]

Measurement of transendothelial electrical resistance (TER)

ECIS 1600R (Applied BioPhysics, Troy, NY, USA) was used to measure the transendothelial resistance (TER) of HDMEC monolayers to assess endothelial barrier integrity as described in detail previously.[33] Endothelial cells were grown to confluence on 8 well arrays (8W10E+; Applied BioPhysics, Troy, NY, USA) and were incubated with fresh medium in the presence or absence of sVE-cadherin^{EC1-5} as indicated below. Additionally, Y27632 and AKB9778 were added simultaneously, when combined with sVE-cadherin^{EC1-5} at the concentrations described above.

Permeability measurements across endothelial monolayers

HDMEC were seeded on top of transwell filter chambers on 12-well plates (0.4 µm pore size; Falcon, Heidelberg, Germany). After reaching confluence, cells were incubated with fresh medium without phenol red (Promocell, Heidelberg, Germany) containing 10 mg/mL FITC-dextran (70 kDa). Paracellular flux was assessed by taking 100 µL aliquots from the outer chamber over 2 h of incubation. Fluorescence was measured using a Tecan Microplate Reader (MTX Lab systems, Bradenton, USA) with excitation and emission at 485 and 535 nm,

respectively. For all experimental conditions, permeability coefficients (P_E) were calculated by the following formula as described previously:[34] $P_E = [(\Delta CA/\Delta t) \times VA]/S \times \Delta CL$, where P_E = diffusive permeability (cm/s), ΔCA = change of FITC-dextran concentration, Δt = change of time, VA = volume of the abluminal medium, S = surface area, and ΔCL = constant luminal concentration.

Immunocytochemistry

Immunostaining was performed as described previously in detail.[34] HDMECs were grown until confluence on cover slips. After incubation with mediators as indicated below fixation with 2% formaldehyde for 10 min was performed. Cells were permeabilized with PBS including 0.1% Triton X-100 (Carl Roth GmbH + Co. KG, Karlsruhe, Germany, 3051.2) for 5 min and blocked in PBS containing 3% bovine serum albumin and 1% normal goat serum (Sigma-Aldrich, Taufkirchen, Germany, A4503 & G0023) at room temperature. Primary antibodies were applied overnight at 4°C. Coverslips were washed four times in PBS and then incubated with secondary antibodies for 1 h at room temperature in present or absence of Alexa Fluor 488 phalloidin (visualization of F-actin 1:60, Invitrogen, A-12379). Coverslips were then mounted using Vectashield HardSet™ with DAPI (Vector Laboratories, Inc.; Burlingame, USA) onto slides for fluorescence microscopy and captured using ZEISS LSM 780 microscope (Carl Zeiss AG, Oberkochen, Germany) and ZEN 3.4 software. Quantification of the images was performed as described in detail below.[35]

Western blotting

Cells growing on 6-well plates were scrapped after adding SDS lysis buffer. Lysates in Laemmli buffer were separated by SDS-PAGE and transferred onto nitrocellulose membranes by wet blotting. Blocking was carried out in 5% low fat milk in Tris-buffered saline Tween-20 (TBST). The membranes were incubated with the appropriate primary antibodies overnight at 4°C. Horseradish peroxidase labelled secondary antibodies were incubated for 1 h at room temperature. Proteins were visualized by the enhanced chemiluminescence technique (ECL, Amersham, Munich, Germany) and developed using ChemiDoc™ Imaging System (BioRad, Feldkirchen, Germany).

Rho GEF-H1 binding assay

For measurements of active Rho GEF-H1 RhoA G17 agarose beads (Abcam, Cambridge, UK, CatNo ab211183) were used according to manufacturer's recommendations. Confluent HDMEC monolayers were lysed and incubated with the agarose beads, incubated for 2h at 4°C. After centrifugation and washing with RIPA buffer, the beads were resuspended in SDS-PAGE sample buffer and boiled for 5 min. The precipitated Rho-GEF was then detected by western blotting using GEF-H1 antibody (abcam, Cambridge, UK, Cat No ab155785). As an internal loading control, untreated equivalent aliquots of confluent HDMEC cells were harvested and western blot using GEF-H1 antibody was performed.

RhoA activity assay

To verify the results obtained from the RhoA G17 agarose beads we used the Rho Activation Assay Biochem Kit (Cytoskeleton, CatNo BK036-S). HDMEC cells were cultivated upto 70% confluence. 24h before harvesting, cells were serum starved. All steps were executed at 4°C and cell lysate were snap frozen. Incubation of cell lysate with rhotekin-RBD beads allows to pulldown GTP-RhoA. To analyse the amount of GPT-bound/activated RhoA, Western Blot was performed using RhoA antibody (kit content).

Proximity ligation assay (PLA)

Cells were seeded on coverslips coated with Collagen IV and treated with sVE-cadherin^{EC1-5} for 24h when reached confluency. Two primary antibodies from different species were selected. Following antibodies were used: mouse anti-VE-cadherin (R&D system) at a dilution of 1:100, rabbit anti-VE-PTP 1:100 (Thermo Fisher). After blocking of unspecific binding sites, slides were incubated with the mentioned primary antibodies. Next, a pair of oligonucleotide-labeled secondary antibodies (PLUS and MINUS Probes) (Duolink Proximity Ligation Assay, Sigma Aldrich, Ref: DUO92101) which bind to the primary antibody were applied. When the PLA probes are in close proximity, connector oligos join the PLA probes and become ligated by addition of ligase at a dilution of 1:40. As a consequence, a closed circle DNA template is formed and acts as a primer for a DNA polymerase. Finally, labeled oligos hybridize to the complementary sequences within the amplicon, which are then visualized as discrete spots (PLA signals) by microscopy analysis.

Atomic force microscopy (AFM) measurements with recombinant VE-cadherin-Fc

AFM measurements were conducted on an atomic force microscope (Nanovizard III, JPK Instruments, Berlin, Germany) mounted on an inverted microscope (IX83, Olympus, Tokyo, Japan). AFM cantilevers (MLCT, Bruker, Calle Tecate, USA) and mica sheets (SPI supplies, West Chester, USA) were functionalized with recombinant VE-cadherin-Fc as outlined earlier.[24] Force-distance curves (FDC) were recorded with an applied force of 0.3 nN, a contact delay of 0.1 s and a retraction velocity of 1 μm/s. For each individual experiment, 1000 FDC were recorded in HBSS to assert baseline VE-cadherin trans-interaction. Thereafter, the mica and cantilever were incubated for 1h with 130 ng/ml sVE-Cad^{EC1-5} and 1000 additional FDC were recorded on the same position on the mica sheet. JPKSPM Data Processing software (JPK Instruments) was used to analyze recorded FDC and to determine VE-cadherin binding events. The resulting binding probability is the ratio of FDC that showed a VE-cadherin interaction and the total number of FDC.

Purification of sVE-cadherin^{EC1-5} supernatant

For all *in vivo* experiments the supernatant of the sVE producing CHO cells were concentrated 10 times via Vivaspin Turbo 15 (4°C, 4000xg). Afterwards the purification was carried out by 60% ammoniumsulfat precipitation. This was done overnight at 4°C on a shaker. After overnight incubation the precipitated protein solution was centrifuged 15 min at 15000 g. The protein was resuspended in NaCl and the dialysis with a 1 kDa molecular weight cut off membrane took two days with several NaCl buffer changes.

Experimental set-up of *in vivo* experiments

We combined established experimental set-ups to allow continuous measurements of microcirculatory flow and capillary leakage using intravital microscopy as well as the simultaneous assessment of macrohaemodynamic parameters to test the effects of sVE-cadherin *in vivo*[4,36–38] in rats.

Prior to 0.8-1.5% (v/v) isofluorane anesthesia (Forene Abbott, Wiesbaden Germany), 0.2 mg/kg BW butorphanol was injected subcutanously. To apply i.v. medication, the right jugular vein was cannulated. Additionally, the left carotid artery was cannulated for continuous blood pressure and heart rate measurements (Hewlett-PackardModel 88S, Hamburg, Germany). Tracheotomy was performed and rats were mechanically ventilated with FiO2 0.28 using a rodent ventilator (Type: 7025, Hugo Sachs Elektronic KG, March-Hugstetten, Germany) in a constant ventilation regime. Animals' body temperature was always kept at 37°C using a heating plate. Sufficient depth of anesthesia under the latter conditions had been tested in preliminary experiments and by estimation of heart rates, mean arterial pressure (MAP), leg movement in response to painful stimuli (which was possible because muscle relaxants were not applied) and eye-lid closing reflex.

Thereafter, median laparotomy was performed, and the mesentery was gently taken out and spread over a pillar as has been described elsewhere.[4] The whole experimental set-up was then carefully placed under a modified inverted Zeiss microscope (Axiovert 200, Carl Zeiss, Göttingen, Germany) equipped with different lenses (Achroplan ×10 NA 0.25/×20 NA0.4/×40 NA 0.6). This allowed continuous observation of microcirculatory flow within postcapillary venules in the mesenteric windows as well as observation of capillary leakage following i.v. injection of FITC-albumin at 5 mg/100 g BW as described below. Images and videos were captured using a digital camera, ColorSnap CF (Photometrics, Tucson, USA), driven by Metamorph analysis software (Molecular Devices GmbH, Biberach a.d. Riss, Germany) and digitally recorded for off-line analysis as described below. In the time course of experiments the upper surface of the mesentery was continuously superperfused with 37.5°C crystalloid solution (Sterofundin, B. Braun Melsung AG, Melsung, Germany).

Randomization of animals into experimental groups

After the preparation procedure animals were allowed to recover for 30 min and then samples for the first blood gas analyses (baseline samples) were taken using an ABL505 blood gas analyser (Radiometer, Copenhagen, Denmark). Each collected amount of blood was replaced by an equal volume of 0.9% sodium chloride (Fresenius Kabi, Bad Homburg, Germany). Before randomization of animals into different groups, the following criteria for exclusion were applied: MAP<60 mmHg, blood loss with Hb<7 g/dl, pH <6.9 or heart rate >550 bpm during preparation procedures. After baseline analyses of blood gas samples and haemodynamic parameters, rats were randomized into experimental groups. One group was used as control group (n=5), in one group (n = 5) 130ng/ml sVE-cadherin^{EC1-5} adapted to the calculated blood volume/BW administered i.v. and one group received 130 ng/ml sVE-cadherin^{EC1-5} 1 h preincubated with VE-PTP inhibitor AKB 9778 (n=5) 0.6 mg per injection subcutaneously as described previously.[13] An additional control group received 2.5 mg/kg BW LPS from *Escherichia coli* (Sigma, L2630; Deisenhofen, Germany) (n = 10) to induce systemic inflammation.[4]

Intravital measurement of microvascular permeability

To assess changes of microvascular permeability during the experimental procedures, digital fluorescence images were taken after single i.v. injection of FITC-albumin 5 mg/100 g BW (Sigma, Deisenhofen, Germany). Fluorescence images were taken using a 100 W mercury lamp and a filter set consisting of a 450–490 nm excitation and a 520 nm emission filter within an inverted microscope (Zeiss Axiovert 200, Carl Zeiss, Göttingen, Germany). Images were taken before randomization, 15 min and 30 min (endpoint) after injection of either NaCl, sVE-cadherin^{EC1-5} or LPS or sVE-cadherin^{EC1-5} + AKB9778. Microvascular permeability was then estimated by determining the extravasation of FITC-albumin by measurements of integrated optical intensity as described previously.[39] The labelled FITC-albumin represented relative changes in permeability: $\Delta I = 1-(Ii-Io)/Ii$, where ΔI is the change in light intensity, Ii is the light intensity inside the vessel, and Io is the light intensity outside the vessel. Grey scale values were measured in the postcapillary venules and in the extravascular space around the venules per unit area throughout the experiments and at selected times using ImageJ software. For each time point 10 randomly selected intravascular and interstitial areas near the postcapillary venules were selected for the measurements by a blinded observer.

Evaluation of microcirculatory flow

Analysis of microvascular blood flow was carried out in straight segments of venular microvessels (20–35 μm in diameter). Velocity of erythrocytes was measured by a blinded investigator using the software VisiView (Puchheim, Germany). For each time point the velocities of 27 randomly chosen erythrocytes within postcapillary venules were measured for each animal. For each time point six to nine vessels per animal were analysed.

Histopathological analyses of lungs

Lungs were removed after experimental procedures for histopathological studies. The tissues were fixed in formaldehyde 3.5% (Otto Fischer, Germany) for more than 24 h. Tissues were then embedded in paraffin and subsequently, sections were stained with H&E for analyses of morphological alterations within the tissues as described previously.[4] BZ-II Analyzer Software was used to measure thickness of alveolar septa. In each of the animals, three sections were analysed and in each section thickness of 15 randomly chosen alveolar septa were measured by a blinded observer.

Quantification of immunostaining

For quantification of staining patterns of junctional proteins ImageJ software was used to randomly collect a total of 30 measurement data per condition from three to four high resolution digital photographs. Measurements were taken at a distance of 10 micrometers to the left and right of the cell border, along an orthogonal line at a 90-degree angle. The resulting data resulted in a graph with a prominent peak in the center of the curve. These measurements included the gray value and the corresponding distance in μm. Subsequently, the collected data was analyzed and graphically represented using the GraphPad software.

For quantification of stress fibers the ImageJ software was used to randomly collect a total of 30 measurement data per condition from three photos out of indepdendent experiments. Measurements were taken at a distance of 10 micrometers right of the cell border at a 90-degree angle. The resulting data produced a graph with a prominent peak in the center of the curve. These measurements included the gray value and the corresponding distance in microns. The collected data was analyzed and graphically represented using the GraphPad software.

Modelling of sVE-cadherin interaction with VE-PTP

3D structures of VE-PTP and VE-Cadherin were extracted from Alphafold databank respectively with P23467 and P33151 cods. Easy version of HADDDOCK online server was used to assess the potential interaction between sVE-cadherin (5^{th} domain) and the 17^{th} domain of VE-PTP. Amino acids with a surface area which exposed to water were more than 40%, were considered as active amino acids. After molecular docking, the output data were divided and the classes were rated based on Z-score. After performing molecular docking and selecting the best complex, the complex was used to do molecular dynamics simulation. To simulate molecular dynamics, the protonation state of ionisable atoms such as aspartate, glutamate, lysine, arginine and histidine at pH7 was first determined using Propka software. Gromacs 2021.5 software was used to simulate molecular dynamics and amber99SB + ILDN force field was used to parameterize the protein. The protein molecule was then placed inside an octagonal box and the distance of the protein from the walls of the box is 0.8 nm. The TIP3P water model added to the box as the solvent. And 4 sodium ions were replaced with water molecules to neutralize the system. The energy of the system was then minimized in 50,000 steps. The steepest descend algorithm was used for minimization. The system temperature then equilibrated to 300 K on the NVT stage for 200 ppm. V-rescale algorithm was used to balance the temperature at this stage. Then, in the NPT stage, the system was stabilized on one Bar pressure with the Parrinello-Rahman algorithm for 200 ps. In the mentioned equilibration steps, heavy protein atoms with a force of 1000 kJ / m2 were kept constant (kJ / mol nm2). In the final stage (production), the simulation was continued under NPT for 100 ns. The time step in all stages of the simulation is 2 fs. The LINCS algorithm was also used to keep the length of covalent bonds (other than hydrogen bonds with heavy atoms) constant. In the production stage, the Nose-Hoover algorithm was used to keep the temperature constant.

QUANTIFICATION AND STATISTICAL ANALYSIS

Statistical analysis was performed using Prism (GraphPad Software, La Jolla, CA, USA). Data are presented as means ± SEM as indicated in the figure legends. Statistical significance was assumed for $p < 0.05$. Paired Student's t-test was performed for two-sample group analysis after checking for a Gaussian distribution. Analysis of variance (ANOVA) followed by Tukey's multiple comparisons test and Bonferroni correction was used for multiple sample groups. For non-parametric data, Kruskal–Wallis following Dunn's post- test or Mann–Whitney U-test were used for significant differences. The tests applied for each of the different experiments are indicated in the figure legends.